Effective Combinatorial Immunotherapy for Castration Resistant Prostate Cancer

Xin Lu[1,6], **James W. Horner**[2], **Erin Paul**[2], **Xiaoying Shang**[1], **Patricia Troncoso**[3], **Pingna Deng**[1], **Shan Jiang**[2], **Qing Chang**[2], **Denise J. Spring**[1], **Padmanee Sharma**[4], **John A. Zebala**[5], **Dean Y. Maeda**[5], **Y. Alan Wang**[1], and **Ronald A. DePinho**[1]

[1]Department of Cancer Biology, The University of Texas MD Anderson Cancer Center, Houston, TX 77030, USA

[2]Institute for Applied Cancer Science, The University of Texas MD Anderson Cancer Center, Houston, TX 77030, USA

[3]Department of Pathology, The University of Texas MD Anderson Cancer Center, Houston, TX 77030, USA

[4]Department of Genitourinary Medical Oncology, The University of Texas MD Anderson Cancer Center, Houston, TX 77030, USA

[5]Syntrix Biosystems, Inc., Auburn, WA 98001

Abstract

A significant fraction of advanced prostate cancer (PCa) patients treated with androgen deprivation therapy (ADT) experience relapse with relentless progression to lethal metastatic castration-resistant prostate cancer (mCRPC)[1]. Immune checkpoint blockade (ICB) using antibodies against cytotoxic-T-lymphocyte-associated protein 4 (CTLA4) or programmed cell death 1/programmed cell death 1 ligand 1 (PD1/PD-L1) generates durable therapeutic responses in a significant subset of patients across a variety of cancer types[2]. However, mCRPC showed overwhelming *de novo* resistance to ICB[3–5], motivating a search for targeted therapies that overcome this resistance. Myeloid-derived suppressor cells (MDSCs) are known to play important roles in tumor immune evasion[6]. Circulating MDSC abundance correlates with PSA levels and metastasis in PCa patients[7–9]. Mouse models of PCa show that MDSCs (CD11b^{+} Gr1^{+}) promote tumor initiation[10]

and progression[11]. These observations prompted us to hypothesize that robust immunotherapy responses in mCRPC may be elicited by the combined actions of ICB agents together with targeted agents that neutralize MDSCs yet preserve T cell function. Here we developed a novel chimeric mouse model of mCRPC to efficiently test combination therapies in an autochthonous setting. Combination of anti-CTLA4 and anti-PD1 engendered only modest efficacy. Targeted therapy against mCRPC-infiltrating MDSCs, using multikinase inhibitors such as cabozantinib and BEZ235, also showed minimal anti-tumor activities. Strikingly, primary and metastatic CRPC showed robust synergistic responses when ICB was combined with MDSC-targeted therapy. Mechanistically, combination therapy efficacy stemmed from the upregulation of IL-1ra and suppression of MDSC-promoting cytokines secreted by PCa cells. These observations illuminate a clinical path hypothesis for combining ICB with MDSC-targeted therapies in the treatment of mCRPC.

Mouse models of PCa engineered with signature mutations of human PCa exhibit autochthonous tumor evolution in an intact immune system[12–14]. However, traditional germline genetic modeling has limited capacity to generate the cohort sizes needed to conduct multi-arm drug testing. This issue is particularly pressing for PCa models based on *PB-Cre*[12] with optimal intercrosses producing 12.5% PCa-prone males (Extended Data Fig. 1a). Here, we employed a novel non-germline mCRPC model in a C57BL/6 background through first establishing JH61 and JH58 mouse embryonic stem cell (mESC) clones (Extended Data Fig. 1b–d) derived from the following genotypes: *PB-Cre$^+$ Pten$^{L/L}$ p53$^{L/L}$ Smad4$^{L/L}$ mTmG$^{L/+}$ LSL-LUC$^{L/+}$* (CPPSML) which exhibited age-dependent GFP$^+$LUC$^+$ PCa development (Fig. 1a). In high percentage chimeras derived from JH61 or JH58 mESCs (Extended Data Table 1a), 50% of mice (4/8 necropsied) developed GFP$^+$ cancer cells at 3 months of age and showed dissemination of cancer cells to draining lymph nodes (LN) and lung (Extended Data Fig. 1e–1f). In prostate, GFP$^+$ areas corresponded to CK8$^+$/CK5$^+$ adenocarcinoma (Extended Data Fig. 1g–h). Importantly, we observed a 4-fold increase in the rate by which PCa-bearing mice can be generated using chimeric modeling (Extended Data Fig. 1a). To study combination therapy targeting mCRPC, we first employed the *PB-Cre$^+$ Pten$^{L/L}$ p53$^{L/L}$ Smad4$^{L/L}$* germline model and demonstrated that an ADT protocol (castration followed by enzalutamide-admixed diet) generated a significant, albeit transient, survival benefit (Extended Data Fig. 2a). Next, CPPSML chimeras were subjected to the same ADT to induce CRPC. To ensure consistency, MRI was used to enroll chimeras with prostate tumor volumes over 150mm^3 before 18 weeks of age – 86/107 (80.4%) chimeras met this criterion (Fig. 1b, Extended Data Fig. 2b). We validated emergence of CRPC in CPPSML chimeras by comparing the response of size-matched primary prostate tumors to ADT in three cohorts: the chimeras, CPPSML mice through breeding, and castration-sensitive *PB-Cre$^+$ Pten$^{L/L}$* mice (Fig. 1c). All treated chimeras succumbed to primary CRPC, with metastases in LN and micrometastases in lungs (Extended Data Fig. 2c). Thus, the CPPSML chimera models provide a speedy platform to test multiple therapies on mCRPC.

Next, mCRPC-bearing chimera mice were enlisted into therapeutic trials. The targeted agents were selected on the basis of (i) strong activity in preclinical PCa models, (ii) initial activity and safety in early phase trials but failure to improve overall survival in Phase III trials of mCRPC, and/or (iii) purported immunomodulatory activities and thus the potential

to enhance or negate ICB. The agents selected were the tyrosine kinase inhibitors dasatinib (Dasa)[15] and cabozantinib (Cabo)[16], and the PI3K/mTOR dual inhibitor BEZ235 (BEZ)[17,18]. Of relevance to this study, previous evidence suggests that PI3K pathway activation in both cancer cells and cancer associated myeloid cells can mediate immunosuppression[19–23] and that BEZ exhibits minimal inhibitory activity on mouse T cells[24]. For ICB, we utilized a cocktail of anti-CTLA4 and anti-PD1 antibodies to maximize the blockade of checkpoint pathways, a regimen in line with a clinical treatment protocol currently being tested in a Phase II trial for mCRPC (NCT02601014). CPPSML chimeras (generated from JH61) with induced and MRI-documented mCRPC were randomized to receive single or combination treatments for 4 weeks before endpoint analysis (Extended Data Fig. 2d). While all targeted agent monotherapies or dual ICB cocktail had minimal impact on prostate tumor weight, the combination of Cabo + ICB or BEZ + ICB showed potent synergistic efficacy in targeting primary and metastatic PCa growth (Fig. 1d–f, Extended Data Fig. 2e). In contrast, ICB alone or Dasa + ICB showed minimal impact on primary or metastatic disease burden, although ICB alone resulted in significant reduction of LN metastasis and lung micrometastasis (Fig. 1d–f, Extended Data Fig. 2e). In a corroborating study with chimeras derived from JH58, Cabo + ICB also generated significant efficacy in the mCRPC setting (Extended Data Fig. 3a–c). At necropsy, Cabo + ICB and BEZ + ICB treated CRPC mice showed minimal residual tumor cells in the prostate (Extended Data Fig. 2e), reduced proliferation and pronounced apoptosis (Extended Data Fig. 3d–g).

We catalogued the constellation of intratumoral immunocytes by CyTOF[11] in the various treatment arms as part of end-point analyses. Continued Dasa, but not Cabo or BEZ, treatment was associated with a significant reduction of tumor infiltrating T cells (Extended Data Fig. 4a), suggesting that the meager impact of Dasa + ICB may reflect depletion of T cells in the tumor microenvironment (TME). This finding is consistent with reported Dasa inhibition of TCR-mediated signal transduction and proliferation[25]. CPPSML PCa tumors predominantly contain granulocytic MDSCs (Gr-MDSCs, $CD11b^+Gr1^+Ly6G^+Ly6C^{low}$) (Extended Data Fig. 4b). Either Cabo or BEZ treatment resulted in a significant reduction of Gr- MDSCs, while ICB alone had no impact (Fig. 2a). However, ICB significantly increased $CD8^+/T_{reg}$ ratio (Fig. 2b), a defining feature for ICB-based therapies. Cabo + ICB and BEZ + ICB further elevated $CD8^+/T_{reg}$ ratios (Fig. 2b). MDSC depletion with anti-Gr1 neutralizing antibody[11] sensitized CRPC in CPPSML to ICB (Extended Data Fig. 4c), arguing that MDSCs mediate *de novo* resistance to ICB and suggesting that Cabo or BEZ enhances ICB through diminishing MDSCs.

To explore the impact of these agents on cells in the TME, *in vitro* viability assays were performed to audit Cabo, BEZ and Dasa activity on MDSCs, $CD8^+$ T cells, and GFP^+ PCa cells harvested from CRPC in CPPSML. Relative to $CD8^+$ T cells and GFP^+ PCa cells, MDSCs displayed a significantly higher sensitivity to Cabo and BEZ, but not to Dasa (Fig. 2c–d, Extended Data Fig. 5a). Similar IC_{50} results were obtained when MDSCs were assayed in medium supplemented with 10ng/ml GM-CSF (Extended Data Fig. 5b) or in medium supplemented with GM-CSF and also pre-conditioned for 12 hours by PCa cell lines established from the CPPSML model (Extended Data Fig. 5c). Moreover, Cabo or BEZ treatment alleviated the suppressive activity of intratumoral MDSCs on $CD4^+$ and $CD8^+$ T

cell proliferation (Fig. 2e, Extended Data Fig. 5d). On the other hand, CD8$^+$ and CD4$^+$ T cell *in vitro* proliferation was only moderately suppressed by Cabo or BEZ, yet completely blocked by Dasa (Fig. 2f–g, Extended Data Fig. 5e). Equivalent drug effects on IFN-γ and IL-2 production by T cells were observed (Fig. 2h–i). In summary, Cabo and BEZ elicited pronounced effect on the infiltration and activity of MDSCs.

Next, phospho-receptor tyrosine kinase (RTK) antibody arrays were used to assess the effect of Cabo and BEZ on the RTK signaling in treated CPPSML tumors (Extended Data Fig. 6a), revealing Cabo-induced downregulation of pEGFR, pErbB2, pErbB3, pAxl, and pPDGFRα, and partial downregulation of pEGFR, pErbB3, and pAxl through indirect effect by BEZ (Fig. 3a). We further observed that Cabo or BEZ also reduced pMET and pVEGFR2 levels, and significantly suppressed PI3K-Akt-mTOR signaling in CPPSML tumors (Fig. 3b). Correspondingly, Cabo or BEZ decreased pS6 signaling in intratumoral Gr1$^+$ MDSCs in the CPPSML TME (Extended Data Fig. 6b–c). These findings raised the possibility that Cabo and BEZ compromise MDSCs through inhibition of PI3K signaling. To test this hypothesis, we sought to rescue the viability of Cabo- or BEZ-treated MDSCs with enforced downstream activation of signaling surrogates. Specifically, MDSCs were isolated from the induced CRPC in CPPSML and co-transfected with recombinant active ERK2 and p70S6K proteins (Fig. 3c). Transfected MDSCs showed improved survival under Cabo or BEZ treatment (Fig. 3d–e). Similar results were obtained when the assay was performed in enhanced medium (Extended Data Fig. 6d–e). These results reinforce the view that Cabo and BEZ exert an impact on the PCa TME in part via selective depletion of MDSCs.

As cytokine signaling plays a pivotal role in the recruitment and activation of MDSCs[6], we further explored the impact of combination treatment on cytokine production in primary CRPC. Cytokine arrays revealed that several key cytokines involved in regulating recruitment and activity of immunosuppressive myeloid cells, including CCL5, CCL12, CD40 and HGF, were reduced by Cabo + ICB or BEZ + ICB treatment. These treatments were also associated with increased IL-1ra, CD142, and VEGF (Fig. 3f, Extended Data Fig. 7a). IL-1ra may contribute to reduced MDSC infiltration[26]. We confirmed that recombinant IL-1ra inhibited IL-1 induced chemoattraction of MDSCs, and this effect was blocked by IL-1ra neutralizing antibody (Fig. 3g). Notably, the cytokine changes were significantly less pronounced in Dasa + ICB treatment (Extended Data Fig. 7b). Noting that cytokine production by cancer cells may influence the functional status of myeloid cells, we cultured MDSCs isolated from CRPC with conditioned medium from the CPPSML PCa cell lines (Extended Data Fig. 7c) and showed upregulated expression of genes responsible for MDSC-induced immune suppression, including *Arg1*, *Cybb*, *Ncf1*, and *Ncf4*[6,11] (Fig. 3h). Critically, the expression induction was largely abolished if the PCa cells were pre-treated with Cabo or BEZ before conditioned medium was collected (Fig. 3i), whereas direct treatment of MDSCs with Cabo or BEZ caused insignificant expression changes (data not shown), suggesting that certain cytokines in the conditioned medium may drive the gene upregulation. Through cytokine array (Extended Data Fig. 7d), we identified 10 cytokines significantly downregulated in the conditioned medium of PCa cells pre-treated with Cabo or BEZ (Fig. 3j), among which CCL5 was also identified as a downregulated cytokine in Cabo + ICB and BEZ + ICB treated CRPC (Fig. 3f). When MDSCs isolated from CRPC tumors were treated with each of the 10 cytokines in the presence of Cabo or BEZ,

significant upregulation of *Arg1*, *Cybb*, *Ncf1* and *Ncf4* was observed with most of the cytokines tested (Extended Data Fig. 7e). Therefore, PCa cells are capable of driving immunosuppression-related gene expression in MDSCs through secretion of multiple cytokines, and this paracrine signaling is impaired by Cabo or BEZ treatment.

BEZ targets multiple p110 isoforms. To test if isoform-specific PI3K inhibitors would generate a comparable level of synergistic advantage when combined with ICB, we tested PI-3065 (p110δ-selective inhibitor[27]) and GSK2636771 (p110β-selective inhibitor[28]). Moreover, given the critical role of Cxcr2 in MDSC recruitment[10,11] and the downregulation of Cxcr2 ligands Cxcl1 and Cxcl2 in the conditioned medium of PCa cells treated with Cabo and BEZ (Fig. 3j), we also tested a novel clinical-stage Cxcr1/2 inhibitor SX-682 (Extended Data Fig. 7f–g) as monotherapy or in combination with ICB in the CPPSML model. Meager to moderate effects of PI-3065, GSK2636771 or SX-682 as single agents on CRPC progression was observed, yet combination with ICB produced strong efficacy (Fig. 4a–b). To further credential our model and assess the pattern of MDSCs in human PCa, a 32-antibody CyTOF panel was developed (Extended Data Table 1b) and used to analyze 12 fresh fine needle biopsy samples from 10 treatment-naïve PCa tumors (Extended Data Table 1c). SPADE analysis displayed the heterogeneous immune cell populations (Extended Data Fig. 8). Results showed the prominence of Gr-MDSCs relative to Mo-MDSCs, with the latter occupying no nodes in the SPADE tree (Fig. 4c). Total T cell load across the samples varied considerably (Fig. 4d), yet the frequency of CD8+ T cells correlated inversely with the frequency of Gr-MDSCs (Fig. 4e), a pattern consistent with the conservation of antagonistic activity of Gr-MDSCs to CD8+ T cells in human PCa.

Here, by using a chimeric model of mCRPC, we showed that ICB alone was insufficient to generate effective response, but a combination of ICB with drugs that inactivate MDSCs demonstrated superior synergistic efficacy against *de novo* resistance to ICB (Extended Data Fig. 9). The differential sensitivity of MDSCs and CD8+ T cells to Cabo, BEZ and possibly other phosphokinase inhibitors should provide an avenue for optimizing the dose and schedule for effective silencing of MDSCs while simultaneously sparing cytotoxic T lymphocytes to attack cancer cells. As with all preclinical model systems and human clinical pathological correlations, prospective clinical trials will be needed to substantiate the hypotheses of our work. Future studies should further explore the combination therapy in the context of both established mCRPC and newly diagnosed PCa together with selective antiandrogens to achieve durable clinical response in this major cancer of men.

Methods

Ethics Statement and Transgenic Mice

All animal work performed in this study was approved by The University of Texas MD Anderson Cancer Center Institutional Animal Care and Use Committee (IACUC). All animals were maintained in pathogen-free conditions and cared for in accordance with the International Association for Assessment and Accreditation of Laboratory Animal Care (AAALAC) policies and certification. All surgeries were performed with isoflurane anesthesia. Analgesic was administered post-surgery along with temperature controlled post-surgical monitoring to minimize suffering. *PB-Cre+ Pten^{L/L} p53^{L/L} Smad4^{L/L}* mice were

described previously[13]. Mice were crossed to *Rosa26-Lox-tdTomato-Lox-EGFP* (*mTmG*) allele[29] (Jackson Laboratory, 007676) and *Rosa26-pCAGGs-LSL-luciferase (LSL-LUC)* allele (MMRRC, 01XAC), both of which were already congenic to C57BL/6, and further backcrossed to C57BL/6 background for four generations. Mice were then intercrossed to obtain "CPPSML" males with homozygous status of *Pten*, *p53* and *Smad4*, heterozygous status of *mTmG and LSL-LUC*, and hemizygous status of *PB-Cre.* To calculate the expected frequency of pups to develop prostate tumors, several factors were included: only males were considered; *PB-Cre* must be transmitted from males to the next generation due to the nonspecific expression in oocytes[30], thus only half of the litter was Cre+; moreover, to circumvent paternal infertility caused by the diseased prostate, the key loxP-flanked tumor suppressor alleles (e.g. *Pten/p53*[31], or Pten/*Smad4*[14]) that are needed for aggressive PCa should be maintained as heterozygous state for the *Pten* loxP allele in the males for continued fertility (*p53* or *Smad4* can be homozygous)[14,32], thus only half of the litter was homozygous for all tumor suppressor alleles. Mice with spontaneous prostate tumors are euthanized at designated time points for tumor collection. Due to the internal status of the tumors, lethargy, reduced mobility and signs of morbidity, rather than maximal tumor size, is used as a protocol-enforced end point.

Mouse Embryonic Stem Cell Derivation

Pten[L/L] *p53*[L/L] *Smad4*[L/L] *mTmG*[L/L] or *Pten*[L/L] *p53*[L/L] *Smad4*[L/L] *LSL-LUC*[L/L] female mice 3–4 weeks old were administered 5iu Pregnant Mare Serum Gonadotropin (PMSG) (NHPP: National Hormone & Peptide Program) via intraperitoneal injection (IP) at 3–4pm. Females were then administered 5iu (IP) Human Chorionic Gonadotropin (hCG) (Sigma-Aldrich, C1063) 46 hours post PMSG and mated 1:1 with *PB-Cre+ Pten*[L/+] *p53*[L/L] *Smad4*[L/L] *LSL-LUC*[L/L] or *PB-Cre+ Pten*[L/L] *p53*[L/L] *Smad4*[L/L] *mTmG*[L/L] male mice, respectively. Successful mating was evaluated and noted by presence of copulus plug 14–16 hours post mating. Blastocyst stage embryos were isolated from those plugged females at embryonic day 3.5 by uterine isolation and flush. Blastocysts were collected and cultured on 16 hour pre-plated inactivated mouse embryonic fibroblasts in pre-equilibrated mES cell culture media. Culture media included Knock-out Serum Replacement (Invitrogen, 10828010), Knock-out DMEM (Invitrogen, 10829-018), Glutamax (Invitrogen, 35050079), Sodium Pyruvate (Invitrogen, 11360-070), Non-essential amino acids (Invitrogen, 11140050), 2-mercaptoethanol (Invitrogen, 21985-023), Pen-Strep (Invitrogen, 15140-122), Insulin (Sigma-Aldrich, 12643), LIF (Millipore, ESG1107), Mitogen activated inhibitor (Stemgent, PD0325901), and Gylcogen synthase kinase inhibitor (Stemgent, CHIR99021). All components were prepared and filter sterilized before use. The culture dish containing the isolated blastocysts was left undisturbed in a water-jacketed copper shelved incubator at 37°C and 5% CO_2. Six days post isolation and culture, mouse embryonic stem cell (mESC) outgrowths were visible and individually picked using Oxford P20 pipet with sterile 100uL round gel filtered tips (USA Scientific, 1022-0810). Each outgrowth was transferred to a well of a sterile 96 well U-bottomed dish containing 15uL sterile PBS. 45uL of 0.25% Trypsin-EDTA (Invitrogen, 25200-056) was added to each well. After a 4-minute incubation at 37°C 5%CO_2, each well was quenched with 300uL of mESC media containing Fetal Bovine Serum (FBS) and pipetted up and down 6–8 times using a multichannel pipet with sterile elongated tips, to generate cell clumps. Individual cell clump populations were transferred to corresponding

wells of a 48 well plate containing 14–16 hour pre-plated mouse embryonic fibroblasts in pre-equilibrated mES cell culture medium. Once the wells reached ~80% confluency they were split to triplicate plates for the purpose of expansion in culture, freezing, and DNA isolation. Generated mES cell lines were genotyped and clones with the genotype *PB-Cre+ Pten^{L/L} p53^{L/L} Smad4^{L/L} mTmG^{L/+} LSL-LUC^{L/+}* (CPPSML) were selected. They were confirmed to be mycoplasma negative, and screened for the presence of the Y chromosome. Chromosome spreads were prepared and observed for abnormalities. Background characterization was performed by SNP analysis.

Chimera Cohort Development

Derived mouse embryonic stem cell lines JH58 and JH61 were genotyped as *PB-Cre+ Pten^{L/L} p53^{L/L} Smad4^{L/L} mTmG^{L/+} LSL-LUC^{L/+}* (CPPSML) and confirmed to contain the Y chromosome. Chimera cohorts were produced by blastocyst microinjection of the mES cells into C57BL/6NTac-Tyr^{tm1Arte} (Taconic, 11971) then followed by uterine implantation into pseudo-pregnant CD-1 (Charles River. 022) or Swiss Webster (Taconic, SW-F) female mice. Specifically, cell lines were cultured to roughly 80% confluence on inactivated mouse embryonic fibroblasts in wells of a 24-well plate in mES cell culture media described above. Cells cultured for the purpose of injection were split 11–16 hours prior to preparation for microinjection. Cells were removed from incubation, washed with sterile PBS and trypsinized with 0.25% Typsin-EDTA. Trypsin was quenched with mES cell culture media containing FBS and the cell culture plate was returned to incubation for 45 minutes to allow the larger mouse embryonic fibroblasts to re-attach to the bottom of the cell culture well. Following that incubation, the desired mES cells were collected and transferred to a 15mL conical tube. The suspension was brought up to 5mL with mESC culture media, gently pipetted up and down to mix and then spun down at 4°C 800 RPM for 4 minutes. All except 100–200uL of media was aspirated from the tube. The bottom of the conical tube was tapped externally to break up the cell pellet and the tube was placed on ice for microinjection use.

C57BL/6NTac-Tyr^{tm1Arte} female mice that had achieved successful strain matched mating post superovulation via timed gonadotropin administration were used as donors for 3.5 day blastocysts. Blastocysts were collected via uterine flush and cultured in M16 medium (Millipore, MR-016-D) overlaid with embryo tested oil in a 35mm culture dish at 37°C 5% CO_2. Blastocysts were each micromanipulated to insert roughly 12 individual mES cells into its blastocoel. Injected blastocysts were then implanted into the uteri of pseudo-pregnant females. Each pseudo-pregnant female received up to 14 micromanipulated blastocysts (up to 7 blastocysts per uterine horn). Chimeras were verified with prostate tumor formation by MRI and enrolled into preclinical studies through randomization which maximized the chance that male mice housed in the same cage received different drugs. Blinding was not applied, because allocation required investigators to assess mouse prostate tumor size with MRI before randomization. Pups were excluded from tumor analysis if they died without significant sign of tumor formation.

SNP Analysis

SNP analysis was performed in the Genetic Services core at MD Anderson Cancer Center. For background characterization of the JH61 ES cell line, 80 microsatellite (SSLP) markers,

polymorphic between FVB/N and 129S6 inbred strains and evenly distributed along the genome (i.e., genome scan), were used as described[33]. In order to analyze the MHC region on mouse chromosome 17, an extra 15 polymorphic SSLPs flanking the H2 complex were added. The results (allelotype) obtained for the SSLP in the H2 region were confirmed by means of H2 PCR-RFLP genotype as described[34].

Noninvasive Mouse and *Ex Vivo* Imaging

For MRI imaging with Bruker ICON, the animals were anesthetized with 1–3% isoflurane and placed on the ICON animal bed. The MRI coil was secured into position over the animal and the entire bed assembly was placed into the Bruker ICON 1T MRI bore. RARE T2 weighted images were acquired in both the coronal and axial planes. After the imaging was completed the animals were recovered under a heating lamp until fully conscious. MRI images were loaded into ImageJ to manually demarcate the contour of the prostate and calculate the total volume. Bioluminescence imaging with IVIS Spectrum was performed as previously described[35]. Fluorescence imaging of dissected prostate tumors, the pair of draining lymph nodes (LNs), and lung was performed with Leica M165FC fluorescence stereomicroscope. LN metastasis score was assigned as 0 (no GFP+ tumor cells), 1 (sparse GFP+ tumor cells on one LN), 2 (sparse GFP+ tumor cells on both LNs, or strong GFP+ tumor cell patches on only one LN), 3 (sparse GFP+ tumor cells on one LNs and strong GFP+ tumor cell patches on the other LN), and 4 (strong GFP+ tumor cell patches on the both LNs). Spontaneous lung micrometastasis was quantified by counting tumor cell clusters with >10 GFP+ tumor cells in each cluster.

Immunohistochemistry, Immunofluorescence and Western Blot

Tissues were fixed in 10% formalin overnight and embedded in paraffin. Immunohistochemical (IHC) and immunofluorescence (IF) staining was performed as previously described[11,14]. IHC slides were scanned with Pannoramic Digital Slide Scanner (3DHISTECH) and images were cropped from virtual slides in Pannoramic Viewer. IF slides were imaged with Nikon A1R Confocal Laser Microscope and quantified with ImageJ. Primary antibodies used include CK5 (Covance, PRB-160P), CK8 (Covance, MMS-162P), Ki67 (Fisher, RM-9106-S1), cleaved caspase 3 (Cell Signaling Technology, 9661), Gr-1 (BioLegend, 108401), phospho-S6 (Cell Signaling Technology, 4858). For Western blot analysis, cells or fresh tissues were lysed on ice using RIPA buffer (Boston BioProducts) supplemented with protease and phosphatase inhibitors (Roche). Western blot procedure was performed as previously described[11,14]. Primary antibodies used include phospho-Met (Cell Signaling Technology, 3077), phospho-VEGFR2 (Cell Signaling Technology, 3770), phospho-Erk1/2 (Cell Signaling Technology, 4370), phospho-Akt (Cell Signaling Technology, 4060), phospho-mTOR (Cell Signaling Technology, 5536), phospho-p70 S6K (Cell Signaling Technology, 9234), phospho-S6 (Cell Signaling Technology, 4856), and vinculin (Millipore, 05-386).

Targeted Pathway Inhibitors

Enzalutamide (MedKoo Biosciences, 201821) was admixed with Purina 5053 Chow at 50 mg drug/kg diet (Research Diets, Inc.), which when fed to mice could reach approximately 10mg/kg/day dose[36] (calculation based on average body weight 25g and daily food intake

5g/day, with online calculator at www.researchdiets.com/resource-center-page/diet-dose-calculator). To induce castration-resistant prostate cancer, mice with confirmed prostate tumor by MRI were surgically castrated and started on Enza-mixed diet for 3 weeks before being moved back to regular chow and treated with therapeutic drugs. For *in vivo* pharmacological inhibition, BEZ235 (Selleck Chemicals, S1009), cabozantinib (Selleck Chemicals, S1119), dasatinib (Selleck Chemicals, S1021), PI-3065 (MedKoo, 407192), GSK2636771 (MedKoo, 205844) were orally administered at daily doses of 45 mg/kg, 30 mg/kg, 30 mg/kg, 50 mg/kg and 30 mg/kg, respectively, daily on a Monday through Friday schedule. SX-682 (Syntrix Biosystems) was orally administered twice a day at 50 mg/kg actual dose on a Monday through Friday schedule. Similar drug dosing methods were described previously[27,28,37–39]. The doses we used for cabozantinib and BEZ235 are clinically relevant: for cabozantinib, to convert the mouse dose into human dose, we calculated 30mg/kg X (1/12.3) = 2.4mg/kg/daily in human (the conversion factor 12.3 can be found in FDA guidance http://www.fda.gov/downloads/Drugs/.../Guidances/UCM078932.pdf, and also in Nair et al[40]). Given a typical human weight of 60kg, the clinical dose range of 60mg/daily (prostate cancer, renal cell carcinoma) to 140mg/daily (medullary thyroid cancer) converts to a human dose range of 1mg/kg/daily to 2.3mg/kg/daily. Therefore, our cabozantinib dose in mice approximates the approved dose for treating medullary thyroid cancer, and is 1.4X higher than used in COMET-1 and COMET-2 Phase III trials of advanced prostate cancer. For BEZ235, previous studies showed that while 300 or 400mg bid (twice daily)[41] showed significant toxicity in patients, 200 mg bid displayed higher tolerability[42]. The dose we used in the mice study, 45mg/kg/daily, is approximately equivalent to 225mg/daily in human, thus is within range of tolerable clinical doses. For immune checkpoint blockade and Gr1 neutralizing antibody treatment, anti-PD1 (clone RMP1-14, BioXcell, BE0146), anti-CTLA4 (clone 9H10, BioXcell, BE0131) or anti-Gr1 (clone RB6-8C5, BioXcell, BE0075) antibodies (or their respective isotype IgG controls) were intraperitoneally administered at 200μg/injection three times/week. The duration of drug treatment was typically 4 weeks before endpoint analysis.

CyTOF of Human Specimens and Mouse Tumors

CyTOF analysis of mouse prostate tumors with data analyzed in FlowJo (Tree Star) followed our previous methods[11]. Human prostate fine needle aspirate specimens were acquired under approved IRB Protocol PA14-0420 at MD Anderson Cancer Center. Informed consent was obtained from all subjects. Prostate tumor single cells were isolated using the Human Tumor Dissociation kit (Miltenyl Biotec, 130-095-929). All isolated cells were depleted of erythrocytes by hypotonic lysis. Cells were blocked with FcR Blocking Reagent (Miltenyl Biotec, 130-059-901) for 10 minutes and incubated with CyTOF antibody mix for 30 minutes at room temperature. Cells were washed once and incubated with Cell-ID™ Cisplatin (Fluidigm, 201064) at 2.5μM for 2.5 minutes for viability staining. Cells were fixed with MaxPar® Fix and Perm Buffer containing Cell-ID™ Intercalator-Ir (Fluidigm, 201192A) at 0.125μM at 4°C overnight to stain the nuclei. The samples were analyzed with CyTOF instrument (Fluidigm) in the Flow Cytometry and Cellular Imaging Core Facility at MD Anderson Cancer Center. Data were analyzed with FlowJo software (Tree Star) and SPADE software[43].

Cell Isolation and *In Vitro* Survival and Migration Assay

Over 95% of all CD11b^{+} Gr1^{+} myeloid cells in established naïve or castration-resistant prostate tumors in CPPSML mice are granulocytic (Ly-6G^{+} Ly-6C[Low]), similar to the level in the *PB-Cre[+] Pten[L/L] Smad4[L/L]* model that we recently reported[11]. Gr-MDSCs were isolated from prostate tumors by first enriching for lymphocytes using Lympholyte-M Cell Separation Media (Cederlane, CL5031) followed by MACS-based isolation using Mouse MDSC Isolation Kit (Miltenyi Biotec, 130-094-538) and plated in RPMI1640 supplemented with 10% FBS and antibiotics. From the same mice, CD8^{+} T cells were isolated from the spleen using Mouse CD8a^{+} T Cell Isolation Kit (Miltenyi Biotec, 130-104-075). MDSCs and CD8^{+} T cells were cultured as described[20]. GFP^{+} prostate cancer cells were isolated from the prostate tumors by FACS sorting with BD FACSAria III Cell Sorter, and cultured in complete DMEM supplemented with 10% FBS and antibiotics. The purity of Gr-MDSCs (CD11b^{+}Gr1^{+}Ly6G^{+}Ly6C^{low}F4/80^{−}), CD8+ T cells (CD3^{+}CD8^{+}) and prostate cancer cells (GFP^{+} Tomato^{-} CD45^{-}) populations was greater than 90% as determined by flow cytometry. Survival assay was performed on 96-well plates with Cell Proliferation Reagent WST-1 (Sigma-Aldrich, 11644807001) as described[20]. Serially diluted drugs (BEZ, Cabo, Dasa) were added to the culture to construct dose-response curves and IC_{50} was calculated with software GraphPad Prism 6. For migration assay, Gr-MDSCs isolated from prostate tumors using MACS technology were added to the upper chamber of a 24-well transwell system (BD Falcon). MDSC short-term culture medium (RPMI1640 supplemented with 10% FBS) with indicated concentration of recombinant mouse IL-1α (BioLegend, 575002), IL-1β (BioLegend, 575102), IL-1ra (VWR, 10006-448) or mouse IL-1ra neutralizing antibody (R&D Systems, AF-480-NA) was added to the bottom chamber. Cells were allowed to migrate to the bottom well for 6 hours at 37°C with 5% CO_2. Migrated cells were fixed and stained with crystal violet for quantification.

T Cell Suppression Assay and Cytokine Production Quantification

T cell suppression assay was performed as we previously described[11] using equal number of MACS-sorted intratumoral Gr-MDSCs and CFSE (Invitrogen) labeled MACS-sorted CD8^{+} or CD4^{+} T cells from spleen of wild type C57BL/6 mice (Jackson Laboratory, 000664). To assess the effect of drugs (BEZ, Cabo, Dasa) on the proliferation of T cells, drugs at different concentrations were added to anti-CD3/anti-CD28 stimulated CFSE-labeled and MACS-sorted CD8^{+} or CD4^{+} T cells from spleen of wild type C57BL/6 mice at time zero. CFSE intensity was quantified 72h later with peaks identified by BD LSRFortessa Cell Analyzer. CFSE peaks indicate the division times. Division times 0, 1-2, ≥3 were defined as No Proliferation, Moderate Proliferation and High Proliferation, respectively. Viable CD4^{+} or CD8^{+} T cells (viability defined as negative DAPI stain) falling in each category were quantified as percentage of total live CD4^{+} or CD8^{+} T cells, respectively. The supernatant medium was used to quantify IFN-γ and IL-2 production by ELISA following manufacturer's manual (BioLegend, 430804 and 431004).

Antibody Array

Mouse prostate tumors treated with defined agents were processed as instructed by manufacturer's protocol and an equal amount (μg) of lysate was used to quantify phospho-

RTK proteins with Proteome Profiler™ Mouse Phospho-RTK Array Kit (R&D Systems, ARY014) or Proteome Profiler Mouse XL Cytokine Array (R&D Systems, ARY028). Medium conditioned by CPPSML PCa cell lines was analyzed with Proteome Profiler Mouse Cytokine Array Kit – Panel A (R&D Systems, ARY006). Quantification of the spot intensity in the arrays was conducted with background subtraction in ImageJ.

Transfection of Recombinant Proteins

MACS-sorted MDSCs isolated from mouse prostate tumors were co-transfected with recombinant active ERK2 (R&D Systems, 1230-KS-010) and p70S6K (R&D Systems, 896-KS-010) following manufacturer's protocol of Chariot Protein Delivery Reagent (Active Motif, 30025). The transfection efficiency was verified to be over 80% in separate wells of MDSCs transfected with β-galactosidase and stained with Beta-Galactosidase Staining Kit (Clontech, 631780). Effect of co-transfection on the resistance of MDSCs to drug treatment was evaluated 12h after transfection with Cell Proliferation Reagent WST-1 (Sigma-Aldrich, 11644807001).

Treatment of MDSCs with Prostate Cancer Cell Conditioned Medium

CPPSML prostate cancer cell lines established and grown in complete DMEM supplemented with 10% FBS were cultured to 90% confluence and renewed with fresh medium followed by medium collection (0.45μm filtered) 12h later. The homozygous deletion of *Pten*, *p53* and *Smad4* were confirmed with genotyping, and all cell lines were confirmed free of mycoplasma with MycoAlert Mycoplasma Detection Kit (Lonza). When the cells were required to be pre-treated with Cabo or BEZ, the renewed medium was supplemented with the drugs at indicated concentration and added to cells. Twelve hours later, conditioned medium was collected with any floating cells removed by 0.45μm filter, and subsequently concentrated 50-fold with Amicon Ultra-15 Centrifugal Filter Unit with Ultracel-3 membrane (Millipore, UFC900324) to deplete small compounds but retain proteins larger than 3kD (including most cytokines). Such concentrated medium was diluted back to 1-fold with complete DMEM. The conditioned medium was used within 12h of collection to culture MACS-sorted MDSCs isolated from mouse prostate tumors. Unconditioned complete DMEM supplemented with 10% FBS was used as negative control. To test if supplementing drug pre-treated conditioned medium with specific cytokines could reverse the effect on MDSCs, the 10 cytokines (all from BioLegend) were added at 100ng/mL individually.

Quantitative RT-PCR

RNA was isolated by RNeasy Kit (Qiagen) and reversed transcribed using Superscript III cDNA synthesis Kit (Life Technology). Quantitative PCR was performed using SYBR-GreenER Kit (Life Technology). The following primers were used: Arg1_F: CTCCAAGCCAAAGTCCTTAGAG; Arg1_R: AGGAGCTGTCATTAGGGACATC; Ncf1_F: ACACCTTCATTCGCCATATTGC; Ncf1_R: TCGGTGAATTTTCTGTAGACCAC; Ncf4_F: GTGAACTCGGCCTGGATCTG; Ncf4_R: AAGCTGCTCAAAGTCGCTCT; Cybb_F: CCTCTACCAAAACCATTCGGAG; Cybb_R: CTGTCCACGTACAATTCGTTCA; internal control Gapdh-F: AGGTCGGTGTGAACGGATTTG; Gapdh_R: TGTAGACCATGTAGTTGAGGTCA.

Preparation of SX-682

SX-682 synthesis was performed at Syntrix Biosystems, Inc. and was described in the patent US 8969365 B2 (Publication date Mar 3, 2015). General chemicals, reagents, and precursors for synthesis were purchased from Sigma-Aldrich (Milwaukee, WI), Boron Molecular (Research Triangle Park, NC), and Frontier Scientific (Logan, UT). Solvents were purchased from either VWR International (West Chester, PA) or Sigma-Aldrich (Milwaukee, WI) and used without further purification. The synthesis steps are described below as illustrated in Extended Data Fig. 7g.

2-Chloro-pyrimidine-5-carboxylic acid **1** (3.16 g, 20 mmol, Frontier Scientific, Logan, UT) was suspended in dichloromethane (40 mL), and oxalyl chloride (3.30 g, 26 mmol) was added, followed by DMF (3 drops) as catalyst. The reaction started to vigorously evolve gas. The reaction was heated to reflux for 1 hour, and then allowed to cool to room temperature. 4-fluoroaniline (2.44 g, 2.2 mmol) was added, vigorous bubbling was seen again, and the reaction mixture warmed up considerably. Triethylamine (4.05 g, 40 mmol) was added, and a flocculent precipitate immediately formed. The reaction mixture was heated to reflux once again for another hour, removed from heat, and stirred at room temperature for 18 hours under nitrogen. The reaction was diluted with EtOAc (100 mL), and the organic layer washed with H_2O, saturated $NaHCO_3$, H_2O, 1N HCl, H_2O, brine, then dried over Na_2SO_4. The liquid was filtered, and evaporated to yield 3.44 g (68%) of the 2-chloro-pyrimidine-5-carboxylic acid (4-fluoro-phenyl)-amide as a light yellow solid. ESI-MS (*m/z*): $[M]^+$ = 252.0. This intermediate was carried forward without further purification.

In a round bottom flask, the intermediate 2-chloro-pyrimidine-5-carboxylic acid (4-fluoro-phenyl)-amide (2.52 g, 10.0 mmol) and anhydrous sodium hydrogen sulfide (1.22 g, 21.8 mmol) were suspended in anhydrous DMF (20 mL). The suspension was stirred at room temperature, and the reaction mixture turned a deep green color. After 1 h, the reaction mixture was partitioned between EtOAc and H_2O, and transferred to a separatory funnel. After the layers were separated, the organic layer was washed twice with a 2:1 mixture of H_2O and 5% aqueous $NaHCO_3$. The combined aqueous layers were acidified with 1 N HCl precipitating a yellow solid. The suspension was left to stand at room temperature for 2 hours, and then the precipitate was collected by vacuum filtration, and rinsed with water. The yellow solid was dried overnight in a vacuum desiccator to yield 2.3 g (92%) of the thiopyrimidinamide intermediate **2**. ^1H NMR (300 MHz, DMSO-d_6) δ 10.29 (s, 1H), 8.77 (bs, 2H), 7.77-7.70 (m, 2H), 7.24 (t, *J* = 8.9 Hz, 2H); ESI-MS (*m/z*): $[M]^+$ = 250.0.

2-Mercapto-pyrimidine-5-carboxylic acid (4-fluoro-phenyl)-amide intermediate **2** (2.32 g, 9.3 mmol) and 2-bromomethyl-4-trifluoromethoxy-phenylboronic acid, pinacol ester (3.85 g, 10.1 mmol, Boron Molecular, Raleigh, NC) were suspended in anhydrous DMF (20 ml). Sonication was used to dissolve the compounds. To the reaction flask triethylamine (2.8 mL, 20.1 mmol, Sigma Aldrich, Milwaukee, WI) was added and a precipitate (triethylamine-HBr) immediately formed. The reaction was layered with nitrogen gas and left to stand at room temperature for 3.75 hr. The reaction was poured into H_2O (500 mL) and layered with EtOAc. The biphasic solution was transferred to a separatory funnel and diluted further with EtOAc and brine. The layers were separated, and the aqueous layer was extracted twice
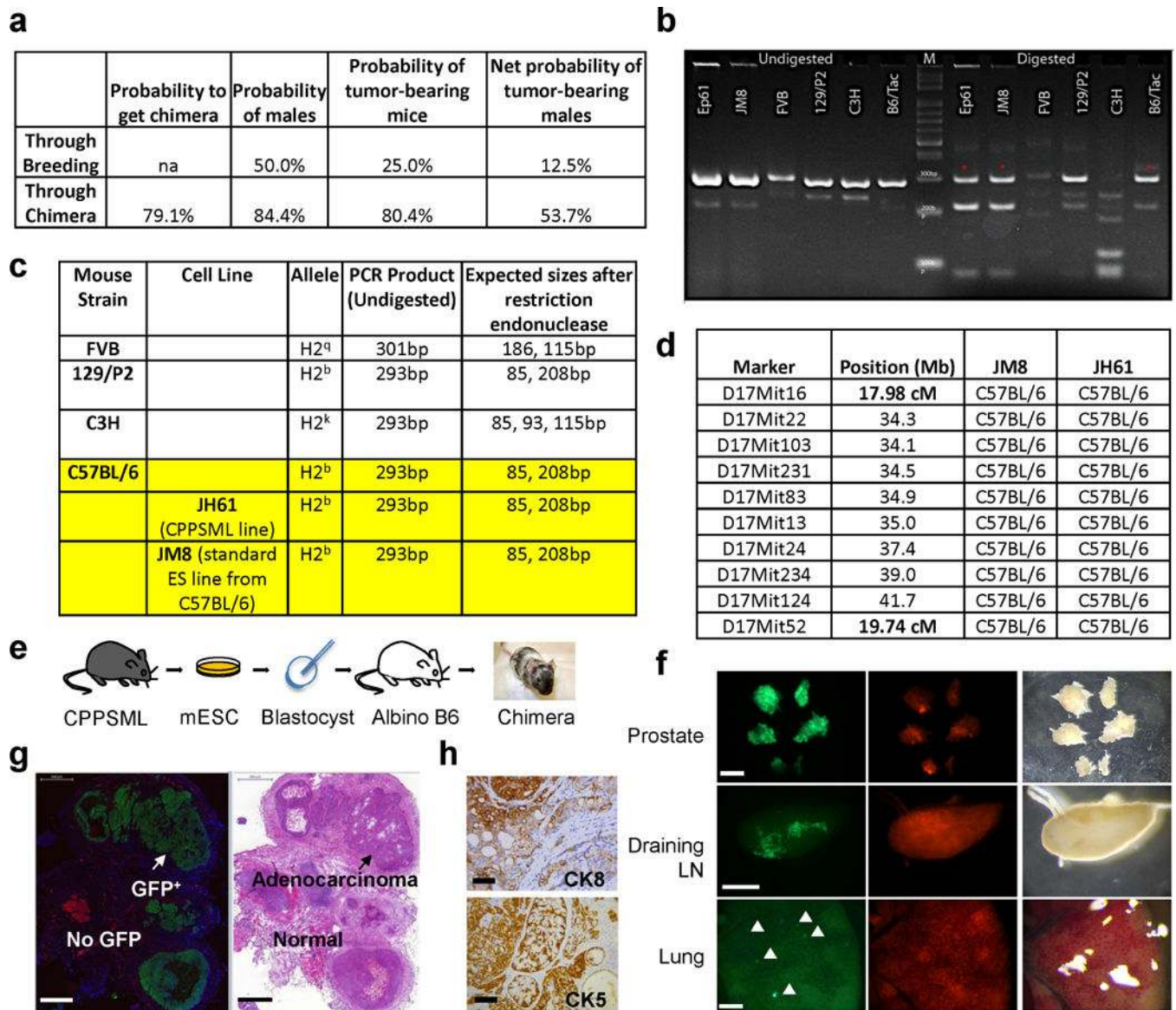
more with EtOAc. The combined organic layers were dried over Na_2SO_4, gravity filtered, and dried by rotary evaporation to yield 5.7 g (98%) of an oil, 2-[2-(4,4,5,5-Tetramethyl-[1,3,2]dioxaborolan-2-yl)-5-trifluoromethoxy-benzylsulfanyl]-pyrimidine-5-carboxylic acid (4-fluoro-phenyl)-amide **3**. ^{1}H NMR (500 MHz, DMSO-d_6) δ 10.52 (s, 1H), 9.11 (s, 2H), 7.81 (d, J = 8.2 Hz, 1H), 7.78-7.75 (m, 2H), 7.55 (s, 1H), 7.28-7.22 (m, 3H), 4.72 (s, 2H), 1.32 (s, 12H); ESI-MS (*m/z*): $[M]^+$ = 550.1. The NMR spectrum also contained peaks consistent with the presence of residual DMF. The intermediate was carried forward without further purification.

The pinacolyl boronate ester was deprotected via hydrolysis of the intermediate trifluoroborate[44]. Compound **3** (5.66 g, 10.3 mmol, 1 eq.) was dissolved in methanol (100 mL). The reaction vessel was charged with 4.5 M aqueous potassium hydrogen fluoride (11.5 mL, 5 eq.) and the resulting solution was stirred for 1 hour. The methanol was removed by rotary evaporation at room temperature and the resulting mixture of yellow and off-white solids was suspended in acetone. The suspension was gravity filtered to remove the insoluble salts, and the resulting clear yellow solution was added via pipette to a flask of H_2O (2 L) and placed in the refrigerator. After cooling for about 1.5 hours, the resulting off-white precipitate was collected by vacuum filtration, rinsing with water. The funnel was dried overnight in a vacuum desiccator to afford 3.87 g (80%) of 2-(2-Boronic acid-5-trifluoromethoxy-benzylsulfanyl)-pyrimidine-5-carboxylic acid (4-fluoro-phenyl)-amide **4** (SX-682). mp = 211- 214 °C; ^{1}H NMR (300 MHz, DMSO-$d6$) δ 10.49 (s, 1H), 9.09 (s, 2H), 8.33 (bs, 2H), 7.78-7.73 (m, 2H), 7.66 (d, J = 8.5 Hz, 1H), 7.46 (s, 1H), 7.25-7.19 (m, 3H), 4.70 (s, 2H); ^{13}C NMR (100.6 MHz, DMSO-d_6) d 173.7, 161.9, 159.8, 157.4, 156.8, 148.8, 144.7, 136.0, 135.7, 135.0, 123.8, 122.3, 122.2, 121.7, 121.4, 118.8, 118.3, 115.5, 115.3, 34.3; ^{19}F NMR (300 MHz, DMSO-$d6$) δ -56.5 (3F), -118.2 (1F); ^{11}B NMR (128.4 MHz, DMSO-$d6$) δ 21.7; HRMS (*m/z*): $[M]^+$ calcd. for $C_{19}H_{15}BF_4N_3O_4S$, 468.0807; found, 468.0803; analysis (calcd., found for $C_{19}H_{14}BF_4N_3O_4S$): C (48.84, 48.91), H (3.02, 3.20), N (8.99, 8.99), S (6.86, 6.73).

Statistical Analysis

Data were presented as mean ± s.d. unless indicated otherwise. Sample size was chosen to ensure 80% power to detect significant effect size based on our recent publications using the transgenic prostate cancer mouse models and thereof derived primary tumor and myeloid cells[11,13,14]. Student's t-test assuming two-tailed distributions or nonparametric Mann-Whitney test was used to calculate statistical significance between groups (no assumption was made that variance was similar between the groups that are being statistically compared). P<0.05 was considered statistically significant.
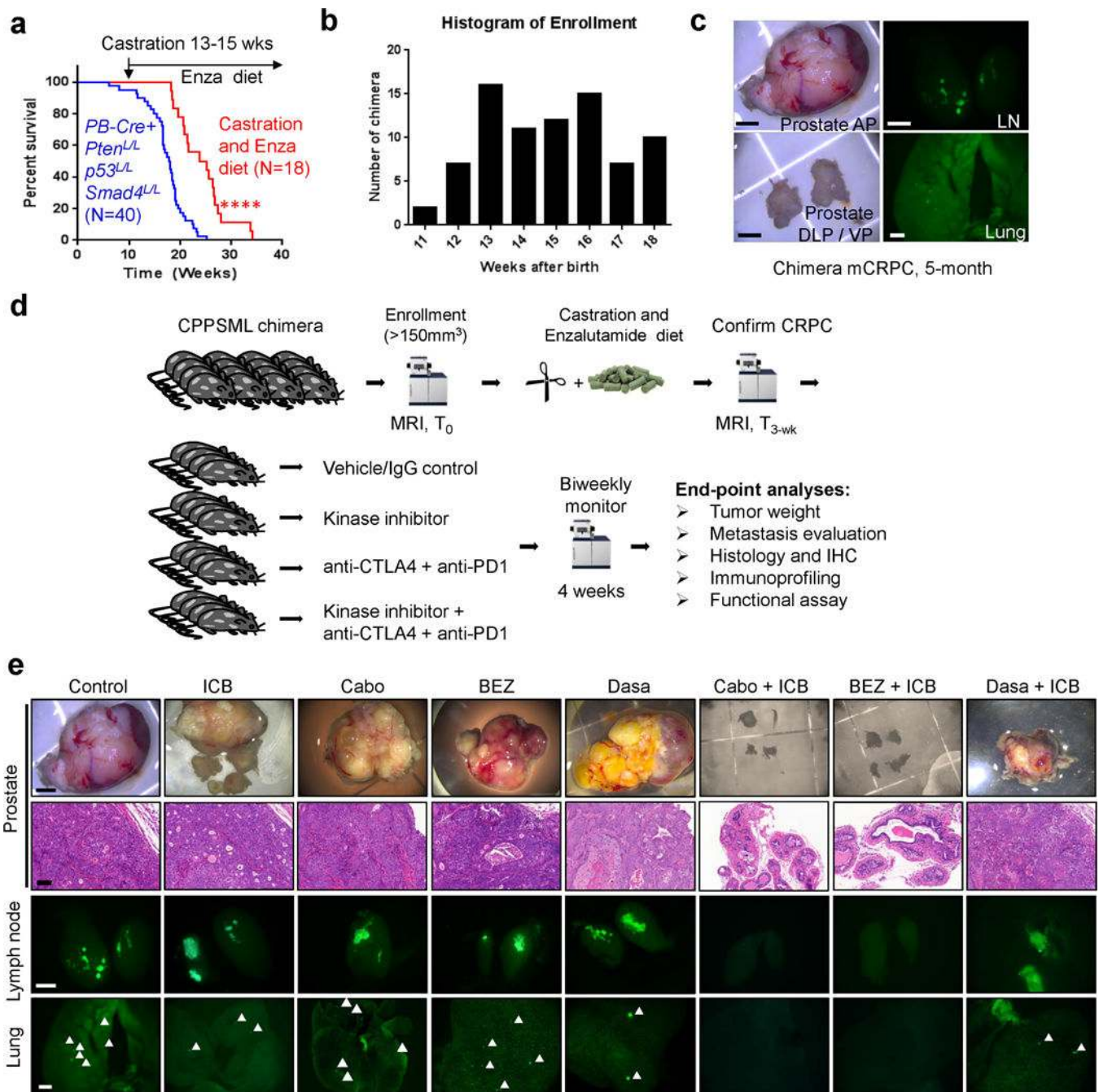
Extended Data

a

	Probability to get chimera	Probability of males	Probability of tumor-bearing mice	Net probability of tumor-bearing males
Through Breeding	na	50.0%	25.0%	12.5%
Through Chimera	79.1%	84.4%	80.4%	53.7%

b

c

Mouse Strain	Cell Line	Allele	PCR Product (Undigested)	Expected sizes after restriction endonuclease
FVB		$H2^q$	301bp	186, 115bp
129/P2		$H2^b$	293bp	85, 208bp
C3H		$H2^k$	293bp	85, 93, 115bp
C57BL/6		$H2^b$	293bp	85, 208bp
	JH61 (CPPSML line)	$H2^b$	293bp	85, 208bp
	JM8 (standard ES line from C57BL/6)	$H2^b$	293bp	85, 208bp

d

Marker	Position (Mb)	JM8	JH61
D17Mit16	17.98 cM	C57BL/6	C57BL/6
D17Mit22	34.3	C57BL/6	C57BL/6
D17Mit103	34.1	C57BL/6	C57BL/6
D17Mit231	34.5	C57BL/6	C57BL/6
D17Mit83	34.9	C57BL/6	C57BL/6
D17Mit13	35.0	C57BL/6	C57BL/6
D17Mit24	37.4	C57BL/6	C57BL/6
D17Mit234	39.0	C57BL/6	C57BL/6
D17Mit124	41.7	C57BL/6	C57BL/6
D17Mit52	19.74 cM	C57BL/6	C57BL/6

e

CPPSML — mESC — Blastocyst — Albino B6 — Chimera

f

g

h

Extended Data Figure 1. Chimeric modeling as an efficient approach to generating spontaneous metastatic prostate cancer

(**a**) Comparison of probability of obtaining PCa-bearing males with CPPSML genotype in a litter, through breeding or chimeric modeling. In chimeric modeling, >75% coat color contributed by injected mESCs is defined as positivity for chimera. (**b–c**) Predicted and experimental results for PCR-RFLP genotyping of H2 locus from several mouse strains and two mESC lines (JM8 as a standard mESC line derived from C57BL/6 strain as control; Ep61 is also known as JH61). Red asterisk in (b) and yellow highlight wells in (c) indicate that the H2 haplotype for JH61 is $H2^b$, same as the C57BL/6 strain. (**d**) SSLP marker analysis of the region on chromosome 17 flanking the H2 complex locus (34-46Mb), showing that JH61 has 100% C57BL/6 background in H2 locus, identical to the standard C57BL/6 mESC line JM8. (**e**) Experimental steps for generating the CPPSML chimeras. (**f**)

Fluorescence images of prostate, draining lymph node (LN) and lung from a representative chimera at 3 months old. GFP$^+$ signals indicate the presence of metastasis to LN and disseminated tumor cells and micrometastasis in lung. Scale bars: prostate 5mm; lymph node and lung, 1mm. (**g**) Fluorescence microscopy and H&E image of snap frozen prostate tumor from chimera showing that the GFP$^+$ area corresponds to adenocarcinoma and the GFP$^-$ area corresponds to normal host cells. Scale bar 500μm. (**h**) IHC staining showing the expansion of both CK8$^+$ luminal lineage and CD5$^+$ basal lineage in the prostate tumor formed in CPPSML chimera. Scale bar 50μm.

Extended Data Figure 2. Experimental design for preclinical therapy of mCRPC in CPPSML chimeras

(**a**) Significant yet transient survival benefit by castration followed by diet admixed with enzalutamide (50mg/kg diet) in *PB-Cre+ Pten^L/L p53^L/L Smad4^L/L* mice (n=40 and 18, respectively). ****$P<0.0001$, Log-rank test. (**b**) Record of enrollment for drug trials showing the time range of prostate tumor formation in the CPPSML chimera. (**c**) Representative CPPSML chimera with primary CRPC, lymph node metastasis, and micrometastasis in lung. Scale bar: prostate 5mm; lymph node and lung, 1mm. AP, DLP and VP denote anterior, dorsolateral and ventral prostate lobes, respectively. (**d**) Experimental

flow for creating mCRPC cohorts and preclinical testing of monotherapy and combination therapy, followed by tumor characterization. (**e**) Representative images of prostate tumors with H&E staining, and GFP$^+$ tumor cells in the lymph node and lung. Scale bar: prostate 5mm; lymph node and lung, 1mm; H&E, 200μm.
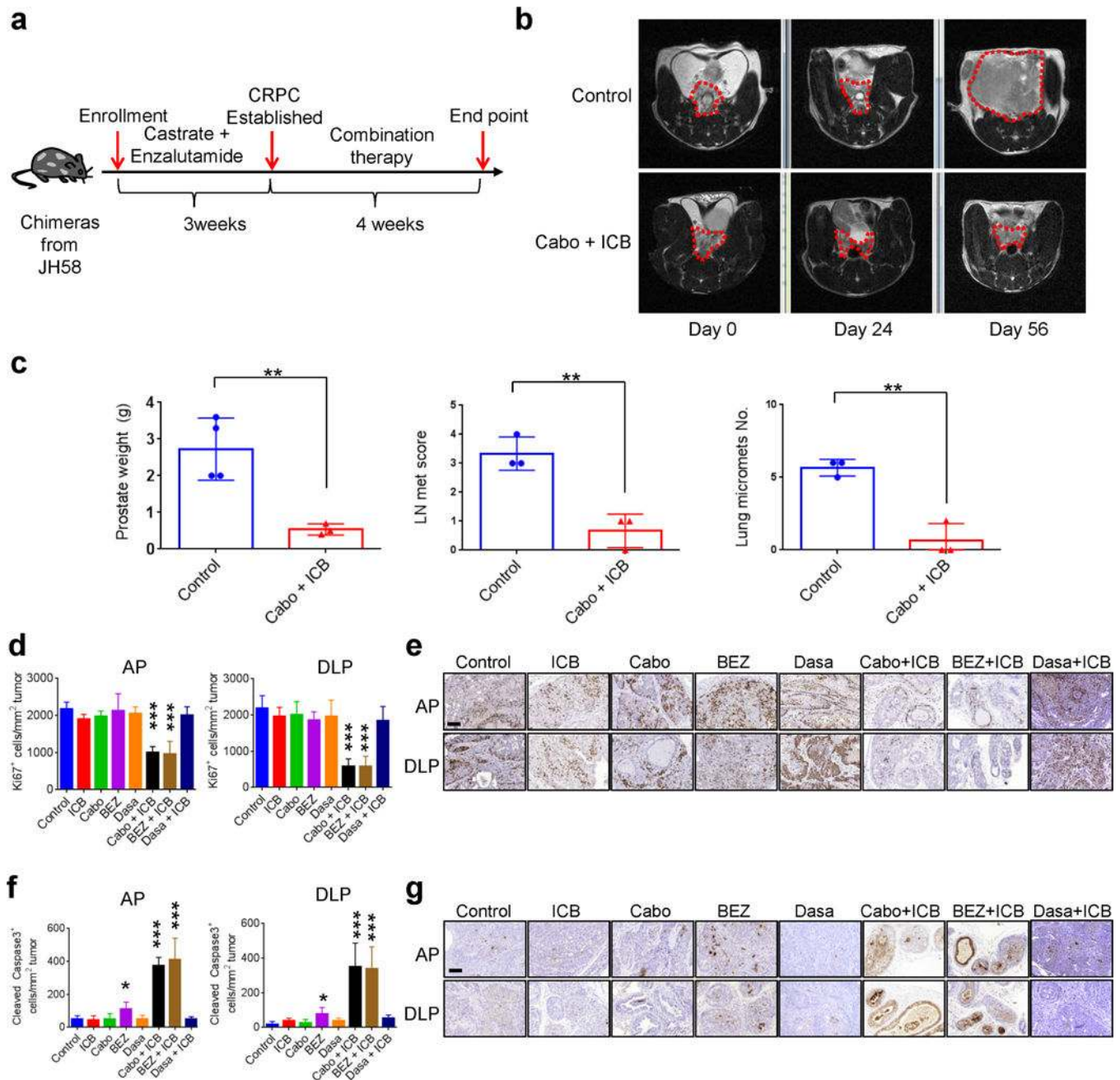
Extended Data Figure 3. Significant combination efficacy by cabozantinib and immune checkpoint blockade observed in chimeras generated from JH58

(**a**) Experimental design for JH58 chimeras, similar to the JH61 chimera experiments. (**b**) Longitudinal MRI images from representative chimeras in control or combination cohorts. Red contour denotes area of prostate tumor. (**c**) Strong anti-tumor effect by combination

therapy in JH58 chimeras shown by prostate tumor weight, lymph node (LN) metastasis score and lung micrometastasis number (n=3, biological replicates). **$P<0.01$, Student's t-test. (**d–e**) Quantification of tumor cell proliferation by Ki67 IHC (n=4, biological replicates) with representative images. Anterior prostate (AP) and dorsolateral prostate (DLP) were quantified separately. (**f–g**) Quantification of tumor cell apoptosis by cleaved caspase 3 (CC3) IHC (n=5, biological replicates) with representative images. Scale bar 100μm. In (c)(d)(f), data represent mean ± s.d. *$P<0.05$, **$P<0.01$, ***$P<0.001$, compared with Control using Student's t-test.
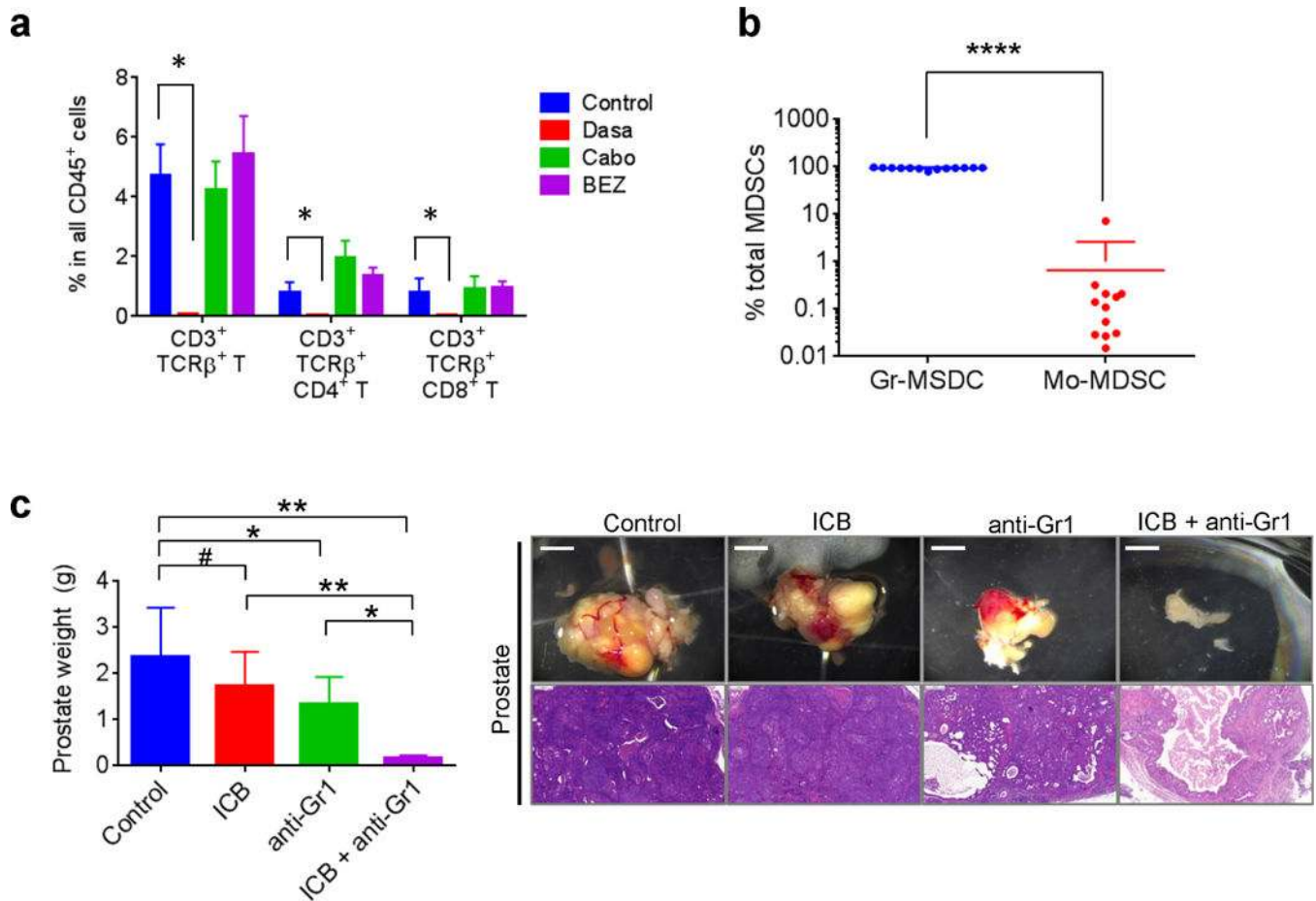
Extended Data Figure 4. Combination efficacy by Gr1 neutralizing antibody with immune checkpoint blockade

(**a**) Dasatinib, but not cabozantinib or BEZ235, significantly reduced the frequency of infiltrating T cells in CRPC of CPPSML mice (n=4, biological replicates). Data represent mean ± s.e.m. *$P<0.05$, Mann-Whitney test. (**b**) Frequency of Gr-MDSCs and Mo-MDSCs in CPPSML prostate tumors (n=13, biological replicates). (**c**) Weight and representative whole organ and H&E images of prostate tumors from CPPSML chimeras induced to develop CRPC and treated with one month of control IgG, ICB (anti-CTLA4 plus anti-PD1 antibodies), anti-Gr1 neutralizing antibody, or combination of ICB and anti-Gr1 (n=4, biological replicates). Scale bars: 3mm for organ images, 200μm for H&E images. In (b) and

(c), data represent mean ± s.d. *P<0.05, **P<0.01, ****P<0.0001, #P>0.05, Mann-Whitney test.
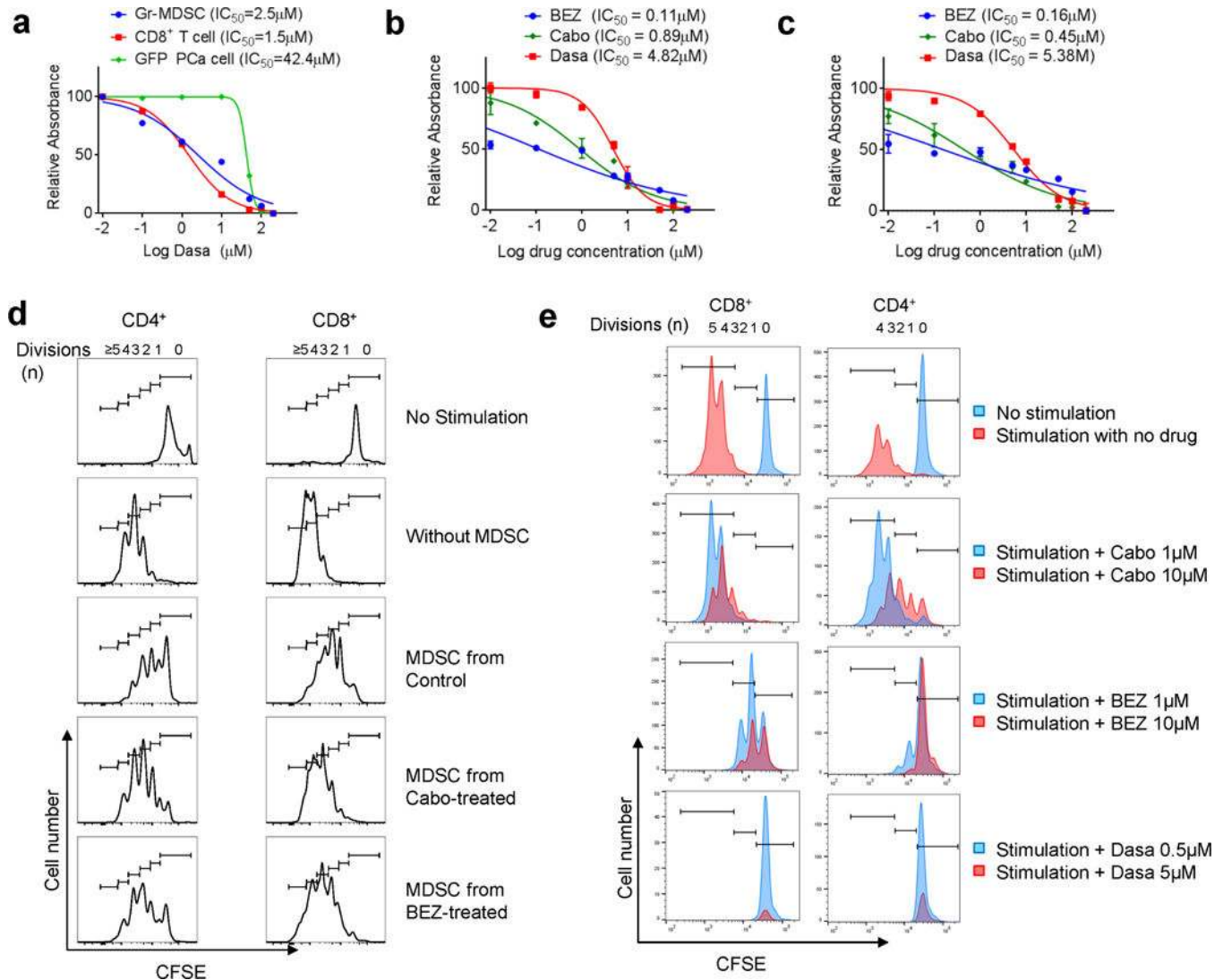
Extended Data Figure 5. Characterization of the effect of drugs on MDSCs
(**a**) Comparison of *in vitro* sensitivity to Dasa by MDSCs, CD8+ T cells, and GFP+ cancer cells isolated from CRPC of CPPSML mice. Cell viability was measured 24h after start of drug treatment using the WST-1 assay. IC_{50} values are indicated. (**b**) Comparison of *in vitro* sensitivity to BEZ, Cabo and Dasa by MDSCs isolated from CRPC of CPPSML mice. The assay was performed in RPMI1640 supplemented with 10% FBS and 10ng/mL GM-CSF (n=2, biological replicates). (**c**) Comparison of *in vitro* sensitivity to BEZ, Cabo and Dasa by MDSCs isolated from CRPC of CPPSML mice. The assay was performed in RPMI1640 supplemented with 10% FBS, 10ng/mL GM-CSF and also pre-conditioned for 12 hours by PCa cell lines established from the CPPSML model (n=2, biological replicates). (**d**) Representative CFSE flow cytometer histograms showing the effect on *in vitro* T cell proliferation by MDSCs isolated from CRPC of CPPSML mice treated with indicated drugs.

Position of CFSE peaks can be used to denote the T cell division times. (**e**) Representative CFSE flow cytometer histograms showing the effect of Cabo, BEZ and Dasa on *in vitro* T cell proliferation.
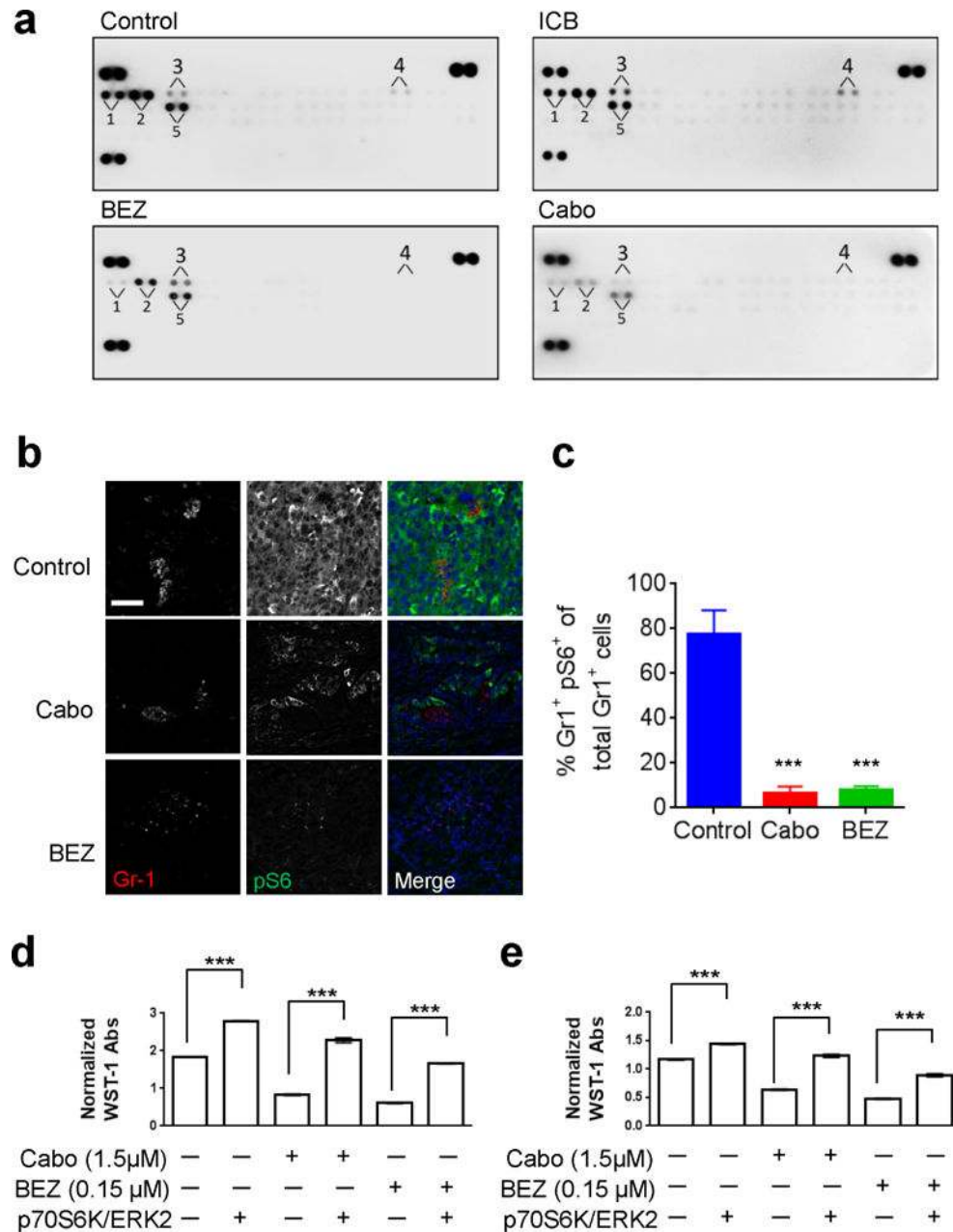
Extended Data Figure 6. Cabozantinib and BEZ235 inhibit PI3K signaling in prostate tumor and intratumoral MDSCs

(**a**) Mouse Phospho-RTK Array measuring phospho-RTK activity in prostate tumors with indicated treatments. 1 through 5 represents p-EGFR, p-ErbB2, p-ErbB3, p-Axl and p-PDGFRα, respectively (n=2, biological replicates). (**b-c**) Reduced phospho-S6 signal in intratumoral MDSCs by Cabo and BEZ treatment, revealed by immunofluorescence co-staining of pS6 and Gr-1 (n=3, biological replicates). Scale bar 100µm. (**d**) WST-1 assay
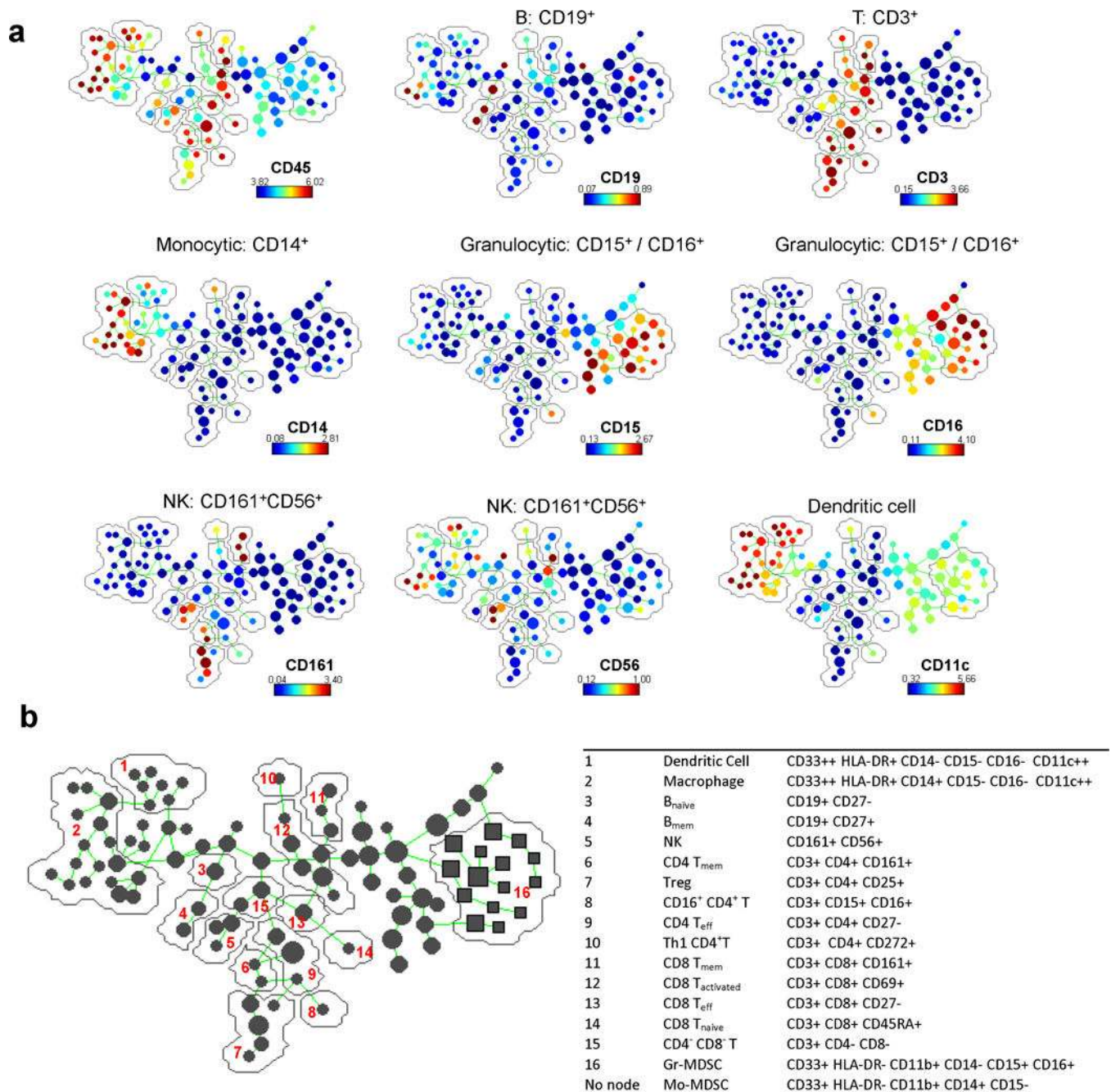
showing that co-transfection of active ERK2 and p70S6K proteins mediated the resistance of MDSCs isolated from CPPSML tumors to the cytotoxicity by Cabo (1.5μM) or BEZ (0.15μM). The assay was performed in RPMI1640 supplemented with 10% FBS and 10ng/mL GM-CSF (n=3, biological replicates). (**e**) WST-1 assay similar as in (d) but performed in RPMI1640 supplemented with 10% FBS, 10ng/mL GM-CSF and also pre-conditioned for 12 hours by PCa cell lines established from the CPPSML model (n=3, biological replicates). In (c)(d)(e), data represent mean ± s.d. ***P<0.001, Student's t-test.
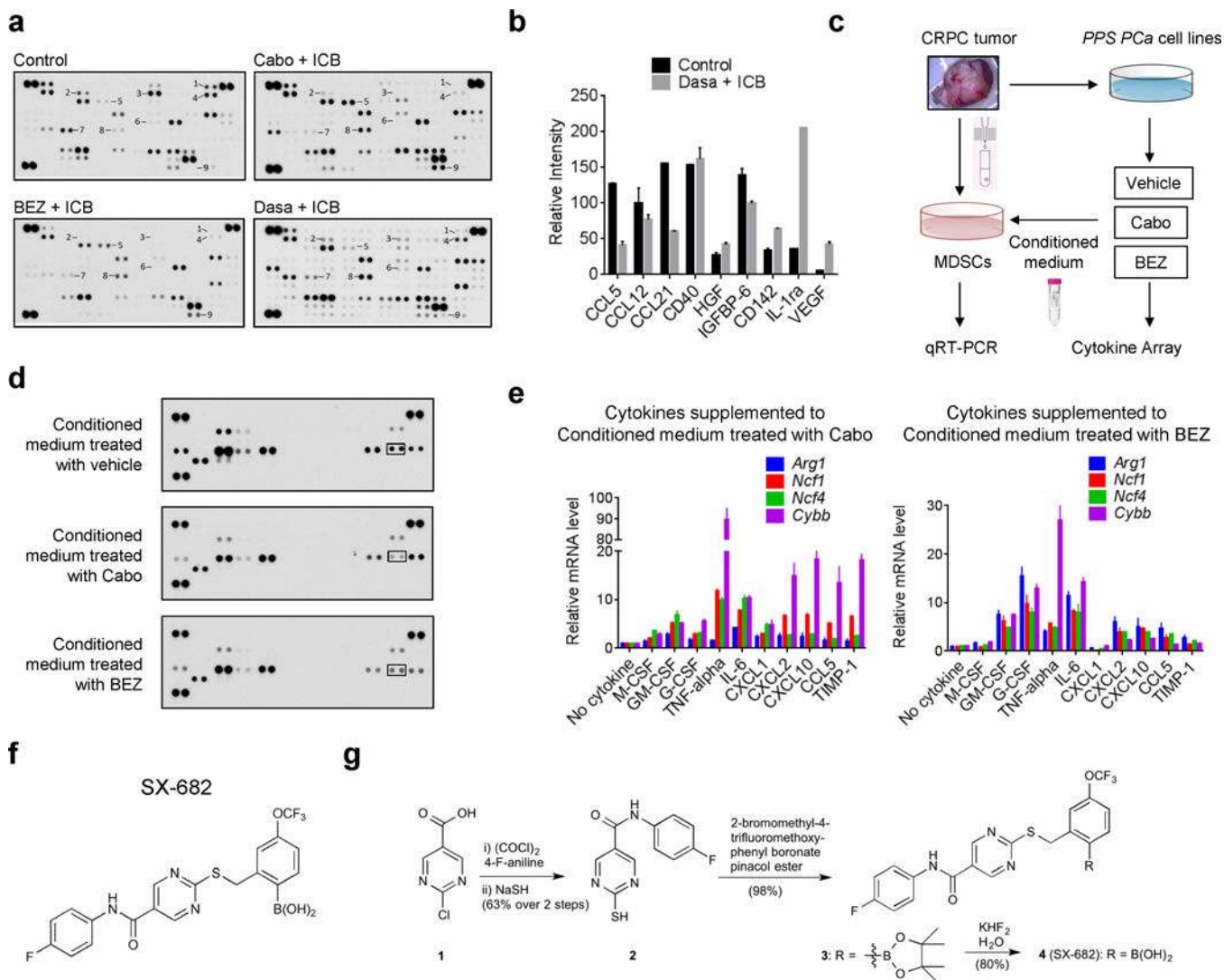
Extended Data Figure 7. Cabozantinib or BEZ235 suppress secretion by prostate cancer cells of several cytokines that promote MDSC activity

(**a**) Quantification of intratumoral cytokine levels in CRPC chimera tumors with indicated treatment using cytokine array (n=2, biological replicates). 1 through 9 represent CCL5, CCL12, CCL21, CD40, CD142, HGF, IGFBP-6, IL-1ra and VEGF, respectively. (**b**) Quantification of intratumoral cytokine levels in Dasa + ICB combination treated CPPSML chimera CRPC with mouse cytokine assay, with image and relative intensity of the numbered cytokines shown (n=2, biological replicates). (**c**) Experimental design for MDSC

culture in the presence of PCa conditioned medium. (**d**) Cytokine array results for conditioned medium from CPPSML PCa cell lines treated with vehicle, Cabo (1μM) or BEZ (1μM) for 12 hours (n=2, biological replicates). Boxed cytokine is CCL5. (**e**) Effect of supplementation of individual cytokines to the conditioned medium from PCa cell lines treated with Cabo (1μM) or BEZ (1μM) on *Arg1*, *Cybb*, *Ncf1* and *Ncf4* from cultured MDSCs (n=3, biological replicates). (**f–g**) Chemical structure and synthesis of allosteric CXCR1/2 antagonist SX-682 (Syntrix Biosystems). For details, please refer to the corresponding session in Methods. In (b)(e)(f), data represent mean ± s.d.

1	Dendritic Cell	CD33++ HLA-DR+ CD14- CD15- CD16- CD11c++
2	Macrophage	CD33++ HLA-DR+ CD14+ CD15- CD16- CD11c++
3	B$_{naive}$	CD19+ CD27-
4	B$_{mem}$	CD19+ CD27+
5	NK	CD161+ CD56+
6	CD4 T$_{mem}$	CD3+ CD4+ CD161+
7	Treg	CD3+ CD4+ CD25+
8	CD16$^+$ CD4$^+$ T	CD3+ CD15+ CD16+
9	CD4 T$_{eff}$	CD3+ CD4+ CD27-
10	Th1 CD4$^+$T	CD3+ CD4+ CD272+
11	CD8 T$_{mem}$	CD3+ CD8+ CD161+
12	CD8 T$_{activated}$	CD3+ CD8+ CD69+
13	CD8 T$_{eff}$	CD3+ CD8+ CD27-
14	CD8 T$_{naive}$	CD3+ CD8+ CD45RA+
15	CD4$^-$ CD8$^-$ T	CD3+ CD4- CD8-
16	Gr-MDSC	CD33+ HLA-DR- CD11b+ CD14- CD15+ CD16+
No node	Mo-MDSC	CD33+ HLA-DR- CD11b+ CD14+ CD15-

Extended Data Figure 8. Detailed cell population annotation in SPADE tree

(**a**) SPADE tree colored by the median intensity of individual markers (indicated above color bar) to facilitate the assignment of tree branches to individual cell populations (shown on the top of each plot) (n=12, biological replicates). (**b**) Surface markers of different immune subpopulations representing small branches of the SPADE tree.
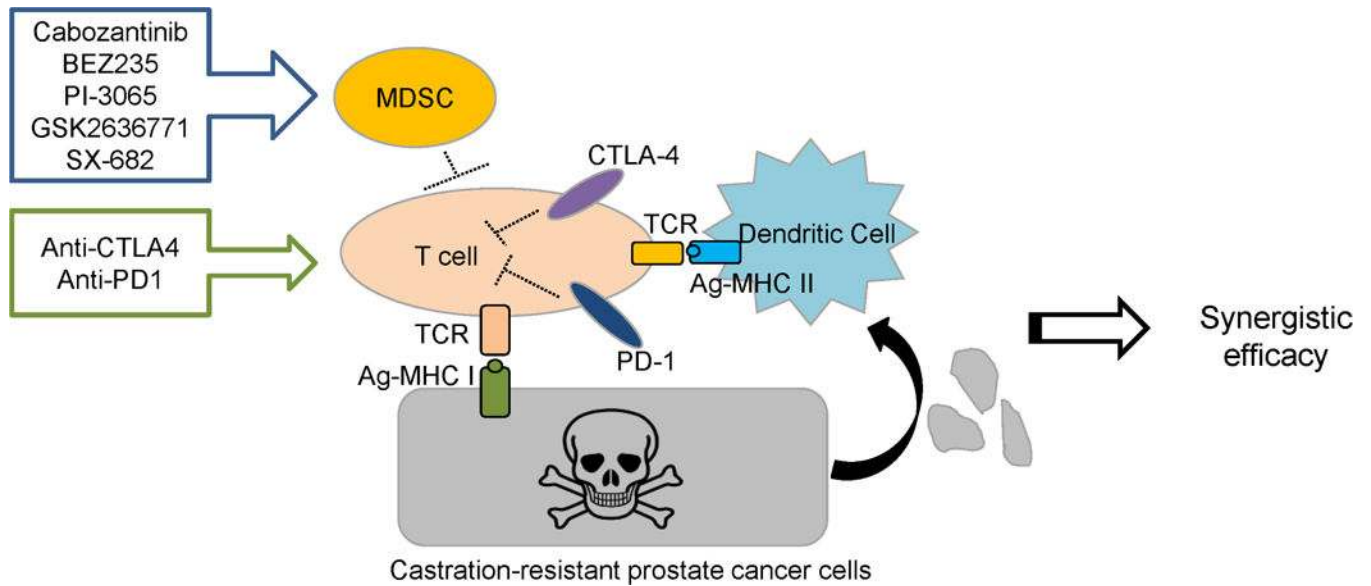
Extended Data Figure 9. Model depicting the combination therapy strategy in treating mCRPC

As demonstrated in the CPPSML chimera model, targeted therapy with agents that inhibit MDSC infiltration frequency and immunosuppressive activity can synergize with ICB to invigorate T cell immunity in the prostate tumor microenvironment thus impair CRPC progression.

Extended Data Table 1
Additional information on mouse model, clinical samples and methodology

(**a**) Coat color chimerism for chimeras derived from JH61. (**b**) CyTOF antibody panel for human prostate tumor samples. (**c**) Clinical information of the fresh fine needle biopsy specimens.

a		
JH61 chimeras	**# chimera**	**Percent**
90–100%	56	48.7
75–90%	35	30.4
50–75%	14	12.2
under 50%	10	8.7
TOTAL	115	100

b				
Marker	**Clone**	**Label**	**Vendor**	**Cat#**
CD19	HIB19	142Nd	DVS-Sunnyvale	3142001B
CD357, GITR	621	143Nd	BioLegend	311602
CD11b	ICRF44	144Nd	DVS-Sunnyvale	3144001B
CD4	RPA-T4	145Nd	DVS-Sunnyvale	3145001B
CD8a	RPA-T8	146Nd	DVS-Sunnyvale	3146001B
CD278, ICOS	C398.4A	147Sm	BioLegend	313502
CD134, OX40	Ber-ACT35	148Nd	BioLegend	350002
CD223, LAG-3	Poly	149Sm	R&D	AF2319
CD202b(Tie2/Tek)	33.1(Ab33)	150Nd	BioLegend	334202
CD123	6H6	151Eu	DVS-Sunnyvale	3151001B
CD137	4-1BB	152Sm	BD	555955
CD133/2	293C3	153Eu	Miltenyi	130-090-851
CD45	HI30	154Sm	DVS-Sunnyvale	3154001B
TIM-3	F38-2E2	156Gd	BioLegend	345002
CD33	WM53	158Gd	DVS-Sunnyvale	3158001B
CD11C	Bu15	159Tb	DVS-Sunnyvale	3159001B
CD161	191B8	161Dy	Miltenyi	191B8 custom
CD69	FN50	162Dy	DVS-Sunnyvale	3162001B
CD45RA	HI100	163Dy	BioLegend	304102
CD15	W6D3	164Dy	DVS-Sunnyvale	3164001B
CD16	3G8	165Ho	DVS-Sunnyvale	3165001B
CD44	BJ18	166Er	DVS-Sunnyvale	3166001B
CD27	O323	167Er	DVS-Sunnyvale	3167002B
CD38	HIT2	168Er	BioLegend	303502
CD25	2A3	169Tm	DVS-Sunnyvale	3169003B
CD3	UCHT1	170Er	DVS-Sunnyvale	3170001B
CD62L	DREG-56	171Yb	BioLegend	304802
CD274, PD-L1	29E.2A3	172Yb	BioLegend	329702
CD14	HCD14	173Yb	BioLegend	325602
HLA-DR	L243	174Yb	DVS-Sunnyvale	3174001B
CD279, PD-1	J105	175Lu	MBL	D133-3
CD56	HCD56	176Yb	DVS-Sunnyvale	3176001B

c				
Patient ID	**Gleason Score (Grades)**	**pStage**	**pN Stage**	**Race**
880709	9(4+5)	pT3b	N0	H
880503	7(3+4)	pT2	N0	W
882696	7(3+4)	pT2	N0	W
883678	7(4+3)	pT2	N0	W
883121	7(4+3)	pT3a	N0	W

c				
Patient ID	**Gleason Score (Grades)**	**pStage**	**pN Stage**	**Race**
882002	9(4+5)	pT3b	N1	W
883318	9(4+5)	pT3b	N0	W
885177	7(4+3)	pT2	N0	A
885567	7(3+4)	pT2	N0	W
885592	7(4+3)	pT2	N0	W

Acknowledgments

References

1. Watson PA, Arora VK, Sawyers CL. Emerging mechanisms of resistance to androgen receptor inhibitors in prostate cancer. Nat Rev Cancer. 2015; 15:701–711. [PubMed: 26563462]

2. Sharma P, Allison JP. The future of immune checkpoint therapy. Science. 2015; 348:56–61. [PubMed: 25838373]

3. Kwon ED, et al. Ipilimumab versus placebo after radiotherapy in patients with metastatic castration-resistant prostate cancer that had progressed after docetaxel chemotherapy (CA184-043): a multicentre, randomised, double-blind, phase 3 trial. The Lancet Oncology. 2014; 15:700–712. [PubMed: 24831977]

4. Beer TM, et al. Randomized, Double-Blind, Phase III Trial of Ipilimumab Versus Placebo in Asymptomatic or Minimally Symptomatic Patients With Metastatic Chemotherapy-Naive Castration-Resistant Prostate Cancer. Journal of Clinical Oncology. 2016

5. Topalian SL. Safety, activity, and immune correlates of anti-PD-1 antibody in cancer. N Engl J Med. 2012; 366:2443–2454. [PubMed: 22658127]

6. Gabrilovich DI, Nagaraj S. Myeloid-derived suppressor cells as regulators of the immune system. Nat Rev Immunol. 2009; 9:162–174. [PubMed: 19197294]

7. Vuk-Pavlović S, et al. Immunosuppressive CD14+HLA-DRlow/- monocytes in prostate cancer. Prostate. 2010; 70:443–455. [PubMed: 19902470]

8. Brusa D, et al. Circulating immunosuppressive cells of prostate cancer patients before and after radical prostatectomy: Profile comparison. Int J Urol. 2013; 2013:12086.

9. Hossain DM, et al. TLR9-Targeted STAT3 Silencing Abrogates Immunosuppressive Activity of Myeloid-Derived Suppressor Cells from Prostate Cancer Patients. Clin Cancer Res. 2015

10. Di Mitri D, et al. Tumour-infiltrating Gr-1+ myeloid cells antagonize senescence in cancer. Nature. 2014; 515:134–137. [PubMed: 25156255]

11. Wang G, et al. Targeting YAP-Dependent MDSC Infiltration Impairs Tumor Progression. Cancer Discov. 2016; 6:80–95. [PubMed: 26701088]

12. Shen MM, Abate-Shen C. Molecular genetics of prostate cancer: new prospects for old challenges. Genes & Development. 2010; 24:1967–2000. [PubMed: 20844012]

13. Ding Z, et al. Telomerase reactivation following telomere dysfunction yields murine prostate tumors with bone metastases. Cell. 2012; 148:896–907. [PubMed: 22341455]

14. Ding Z, et al. SMAD4-dependent barrier constrains prostate cancer growth and metastatic progression. Nature. 2011; 470:269–273. [PubMed: 21289624]

15. Araujo JC, et al. Docetaxel and dasatinib or placebo in men with metastatic castration-resistant prostate cancer (READY): a randomised, double-blind phase 3 trial. The Lancet Oncology. 2013; 14:1307–1316. [PubMed: 24211163]

16. Smith M, et al. Phase III Study of Cabozantinib in Previously Treated Metastatic Castration-Resistant Prostate Cancer: COMET-1. Journal of Clinical Oncology. 2016

17. Carver, Brett S., et al. Reciprocal Feedback Regulation of PI3K and Androgen Receptor Signaling in PTEN-Deficient Prostate Cancer. Cancer Cell. 2011; 19:575–586. [PubMed: 21575859]

18. Jia S, et al. Opposing effects of androgen deprivation and targeted therapy on prostate cancer prevention. Cancer Discov. 2013; 3:44–51. [PubMed: 23258246]

19. Peng W, et al. Loss of PTEN Promotes Resistance to T Cell-Mediated Immunotherapy. Cancer Discov. 2016; 6:202–216. [PubMed: 26645196]

20. Kim K, et al. Eradication of metastatic mouse cancers resistant to immune checkpoint blockade by suppression of myeloid-derived cells. Proceedings of the National Academy of Sciences. 2014; 111:11774–11779.

21. Rivera, Lee B., et al. Intratumoral Myeloid Cells Regulate Responsiveness and Resistance to Antiangiogenic Therapy. Cell Reports. 2015; 11:577–591. [PubMed: 25892230]

22. De Henau O, et al. Overcoming resistance to checkpoint blockade therapy by targeting PI3Kγ in myeloid cells. Nature. 2016; 539:443–447. [PubMed: 27828943]

23. Kaneda MM, et al. PI3Kγ is a molecular switch that controls immune suppression. Nature. 2016; 539:437–442. [PubMed: 27642729]

24. Frick A, et al. Immune cell-based screening assay for response to anticancer agents: applications in pharmacogenomics. Pharmacogenomics and personalized medicine. 2015; 8:81–98. [PubMed: 25897258]

25. Schade AE, et al. Dasatinib, a small-molecule protein tyrosine kinase inhibitor, inhibits T-cell activation and proliferation. Blood. 2008; 111:1366–1377. [PubMed: 17962511]

26. Tu S, et al. Overexpression of Interleukin-1β Induces Gastric Inflammation and Cancer and Mobilizes Myeloid-Derived Suppressor Cells in Mice. Cancer Cell. 2008; 14:408–419. [PubMed: 18977329]

27. Ali K, et al. Inactivation of PI(3)K p110[dgr] breaks regulatory T-cell-mediated immune tolerance to cancer. Nature. 2014; 510:407–411. [PubMed: 24919154]

28. Costa C, et al. Measurement of PIP3 Levels Reveals an Unexpected Role for p110β in Early Adaptive Responses to p110α-Specific Inhibitors in Luminal Breast Cancer. Cancer Cell. 2015; 27:97–108. [PubMed: 25544637]

29. Muzumdar MD, Tasic B, Miyamichi K, Li L, Luo L. A global double-fluorescent Cre reporter mouse. Genesis. 2007; 45:593–605. [PubMed: 17868096]

30. Birbach A. Use of PB-Cre4 Mice for Mosaic Gene Deletion. PLoS ONE. 2013; 8:e53501. [PubMed: 23308238]

31. Chen Z, et al. Crucial role of p53-dependent cellular senescence in suppression of Pten-deficient tumorigenesis. Nature. 2005; 436:725–730. [PubMed: 16079851]

32. Ding Z, et al. Telomerase Reactivation following Telomere Dysfunction Yields Murine Prostate Tumors with Bone Metastases. Cell. 2012; 148:896–907. [PubMed: 22341455]

33. Benavides F, et al. Microsatellite DNA variants between the inbred SENCAR mouse strains. Molecular carcinogenesis. 2000; 28:191–195. [PubMed: 10972988]

34. Saha BK. Typing of murine major histocompatibility complex with a microsatellite in the class II Eb gene. J Immunol Methods. 1996; 194:77–83. [PubMed: 8690943]

35. Lu X, et al. VCAM-1 Promotes Osteolytic Expansion of Indolent Bone Micrometastasis of Breast Cancer by Engaging α4β1-Positive Osteoclast Progenitors. Cancer Cell. 2011; 20:701–714. [PubMed: 22137794]

36. Asangani IA, et al. Therapeutic targeting of BET bromodomain proteins in castration-resistant prostate cancer. Nature. 2014; 510:278–282. [PubMed: 24759320]

37. Maira SM, et al. Identification and characterization of NVP-BEZ235, a new orally available dual phosphatidylinositol 3-kinase/mammalian target of rapamycin inhibitor with potent in vivo antitumor activity. American Association for Cancer Research. 2008; 7:1851–1863.

38. Nguyen HM, et al. Cabozantinib Inhibits Growth of Androgen-Sensitive and Castration-Resistant Prostate Cancer and Affects Bone Remodeling. PLoS ONE. 2013; 8:e78881. [PubMed: 24205338]

39. Vitali R, et al. Activity of tyrosine kinase inhibitor Dasatinib in neuroblastoma cells in vitro and in orthotopic mouse model. International Journal of Cancer. 2009; 125:2547–2555. [PubMed: 19623650]

40. Nair A, Jacob S. A simple practice guide for dose conversion between animals and human. Journal of Basic and Clinical Pharmacy. 2016; 7:27–31. [PubMed: 27057123]

41. Fazio N, et al. A Phase II Study of BEZ235 in Patients with Everolimus-resistant, Advanced Pancreatic Neuroendocrine Tumours. Anticancer Res. 2016; 36:713–719. [PubMed: 26851029]

42. Carlo MI, et al. A Phase Ib Study of BEZ235, a Dual Inhibitor of Phosphatidylinositol 3-Kinase (PI3K) and Mammalian Target of Rapamycin (mTOR), in Patients With Advanced Renal Cell Carcinoma. Oncologist. 2016; 21:787–788. [PubMed: 27286790]

43. Bjornson ZB, Nolan GP, Fantl WJ. Single-cell mass cytometry for analysis of immune system functional states. Current opinion in immunology. 2013; 25:484–494. [PubMed: 23999316]

44. Yuen AKL, Hutton CA. Deprotection of pinacolyl boronate esters via hydrolysis of intermediate potassium trifluoroborates. Tetrahedron Letters. 2005; 46:7899–7903.
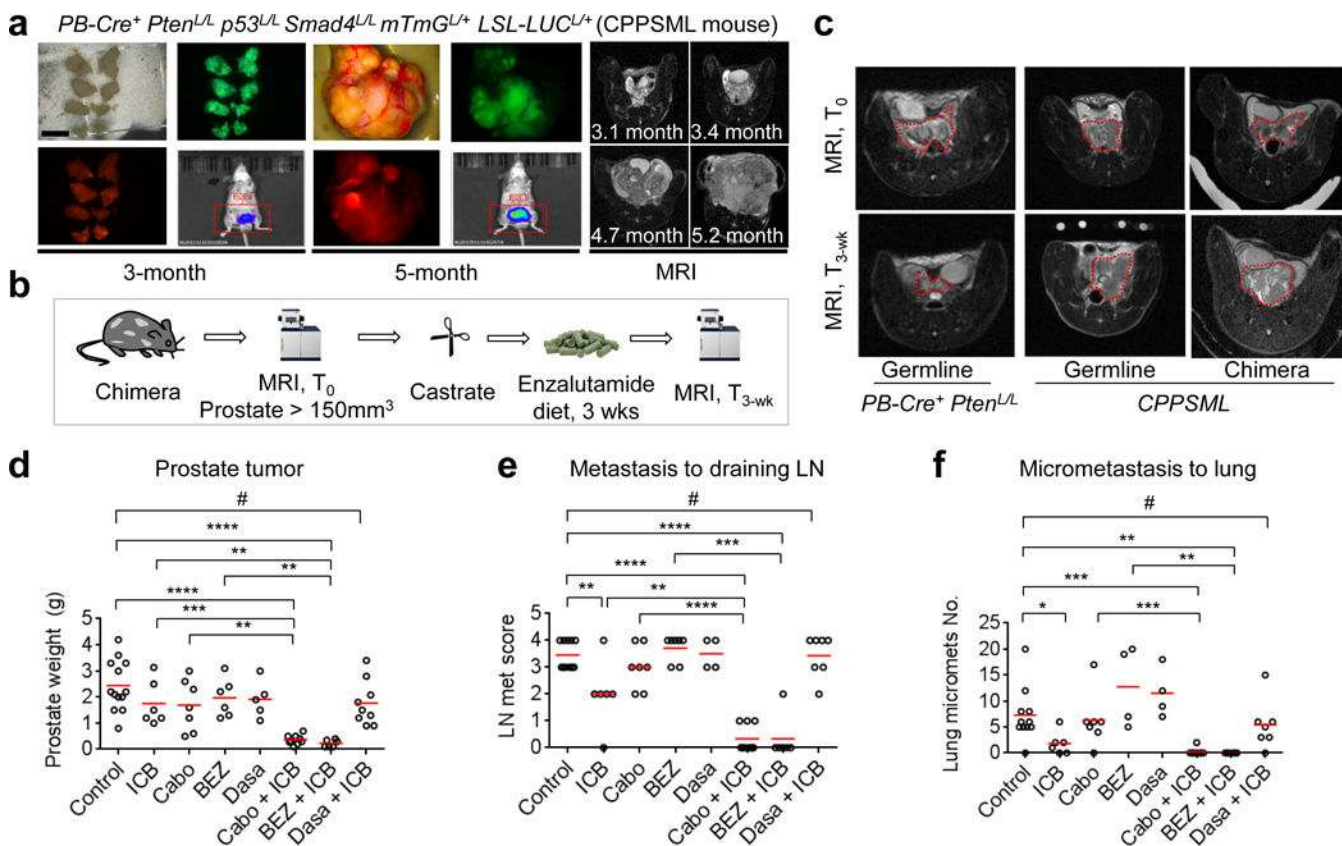
Figure 1. Strong combination synergy by immune checkpoint blockade with cabozantinib or BEZ235 in mCRPC

(**a**) Spontaneous prostate tumor development in the CPPSML model with tumors detected by fluorescence, bioluminescence and MRI. Scale bar 5mm. (**b-c**) Procedures and representative MRI images for testing prostate tumor response to castration and enzalutamide diet in *PB-Cre+ PtenL/L* mice and CPPSML mice (n=5, biological replicates). (**d-f**) Preclinical trial results of prostate tumor weight, lymph node (LN) metastasis score and lung micrometastasis number (n=11, 6, 7, 4, 4, 9, 6, and 7 respectively, biological replicates). Red bar indicates the mean. *$P<0.05$, **$P<0.01$, ***$P<0.001$, ****$P<0.0001$, #$P>0.05$, Mann-Whitney test.
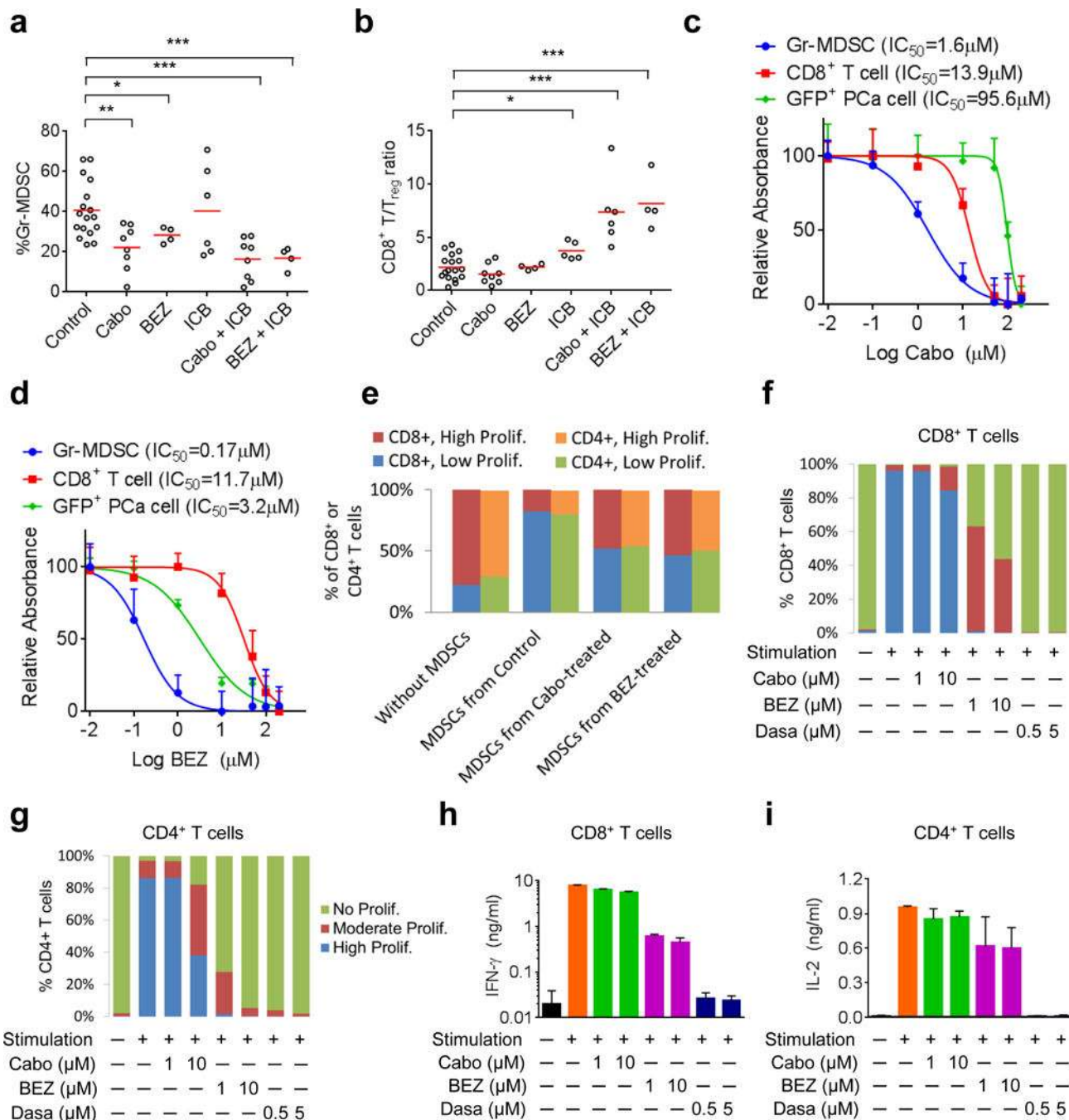
Figure 2. Cabozantinib and BEZ235 attenuate MDSC frequency and immunosuppressive activity in the tumor microenvironment

(**a–b**) CyTOF quantification of intratumoral Gr-MDSC frequency and CD8$^+$ T/T$_{reg}$ ratio by indicated treatments (n=17, 8, 4, 6, 8 and 4, respectively). Red bar indicates the mean. *P<0.05, **P<0.01, ***P<0.001, Mann-Whitney test. (**c-d**) *In vitro* sensitivity to Cabo (c) and BEZ (d) by MDSCs, CD8$^+$ T cells, and GFP$^+$ cancer cells isolated from CRPC in CPPSML mice with IC$_{50}$ indicated (n=3, biological replicates). (**e**) T cell proliferation assay when co-cultured 1:1 with MDSCs isolated from control- or drug-treated CRPC. High and

Low Proliferation was defined as T cell division $\geq$3 and $\leq$2, respectively (n $\geq$4, biological replicates). (**f-g**) Drug effect on CD8$^+$ (f) and CD4$^+$ (g) T cell proliferation assay. High, Moderate and No Proliferation was defined as T cell division $\geq$3, $\leq$2 and =0, respectively (n=3, biological replicates). (**h-i**) Drug effect on IFN-γ secretion (by CD8$^+$ T cells) and IL-2 secretion (by CD4$^+$ T cells) in the assay in (f-g), measured by ELISA (n=3, biological replicates). In (c-d)(h-i), data represent mean ± s.d.
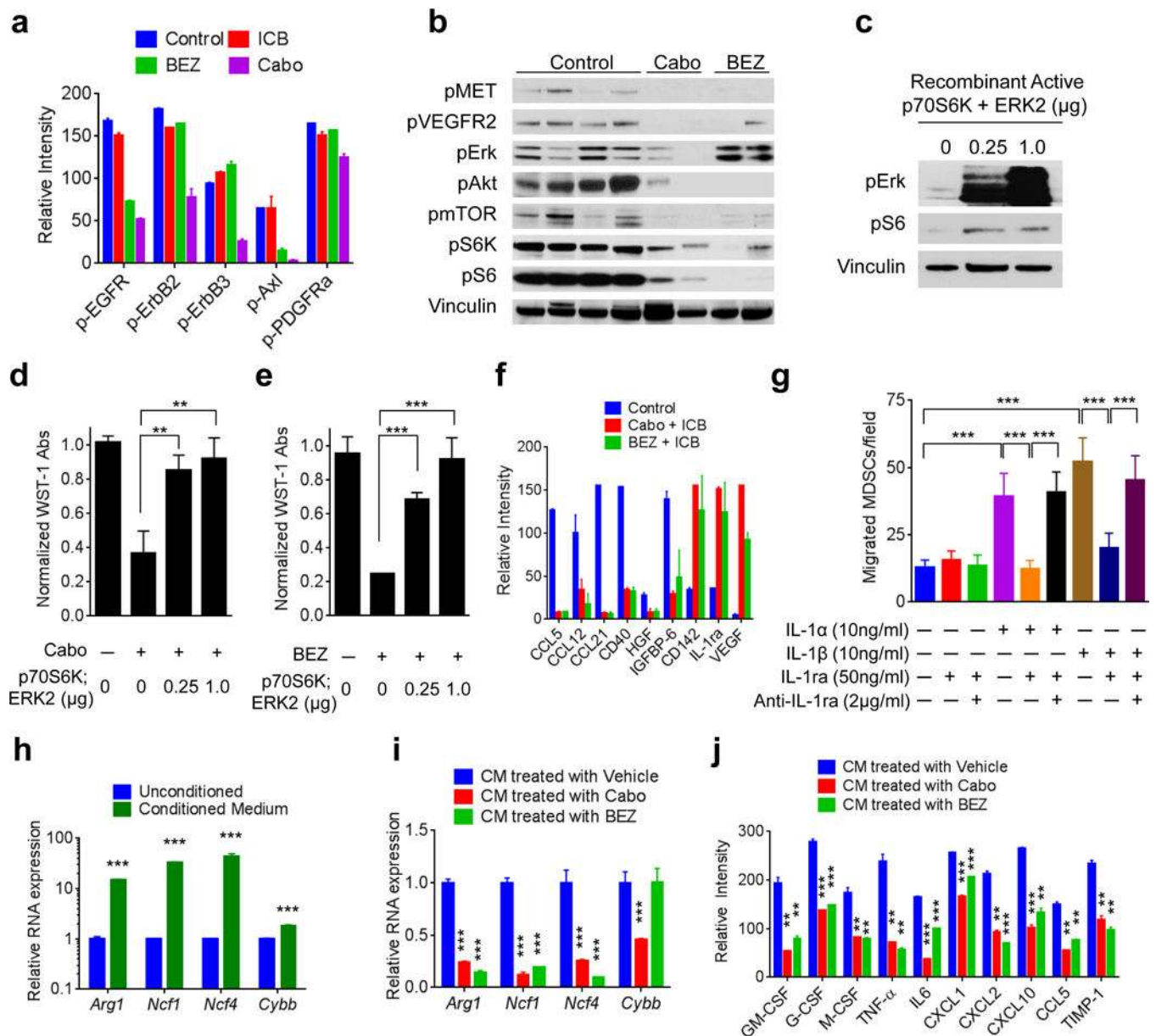
Figure 3. Cabozantinib and BEZ235 inhibit PI3K signaling and modulate MDSC-regulating cytokines

(**a**) Relative phospho-RTK intensity measured with phospho-RTK array for treated CRPC (n=2, biological replicates). (**b**) Level of phospho-proteins in RTK and PI3K/Akt/mTOR pathways in treated tumors, detected with western blot. (**c**) Phospho-Erk and phospho-S6 intensity in MDSCs when co-transfected with ERK2 and p70S6K, detected with western blot. (**d-e**) Effect of ERK2 and p70S6K on the resistance of MDSCs to Cabo (1.5μM) or BEZ (0.15μM), measured with WST-1 assay (n=3, biological replicates). (**f**) Quantification of tumor cytokine levels in treated CRPC using cytokine array (n=2, biological replicates). (**g**) Transwell MDSC migration assay (n=3, biological replicates). (**h**) RNA expression levels of indicated genes by intratumoral MDSCs when cultured in conditioned medium by CPPSML PCa cell lines, measured with qRT-PCR (n=3, biological replicates). (**i**) Effect on

gene expression by pretreating CPPSML PCa cells with Cabo and BEZ before conditioned medium was collected to culture MDSCs (n=3, biological replicates). (**j**) Quantification of cytokine levels in conditioned medium from CPPSML PCa cell lines pretreated with vehicle, Cabo (1μM) or BEZ (1μM), measured with cytokine array (n=2, biological replicates). In (a) (d-j), data represent mean ± s.d. **P<0.01, ***P<0.001, Student's t-test. For gel source data, see Supplementary Figure 1.
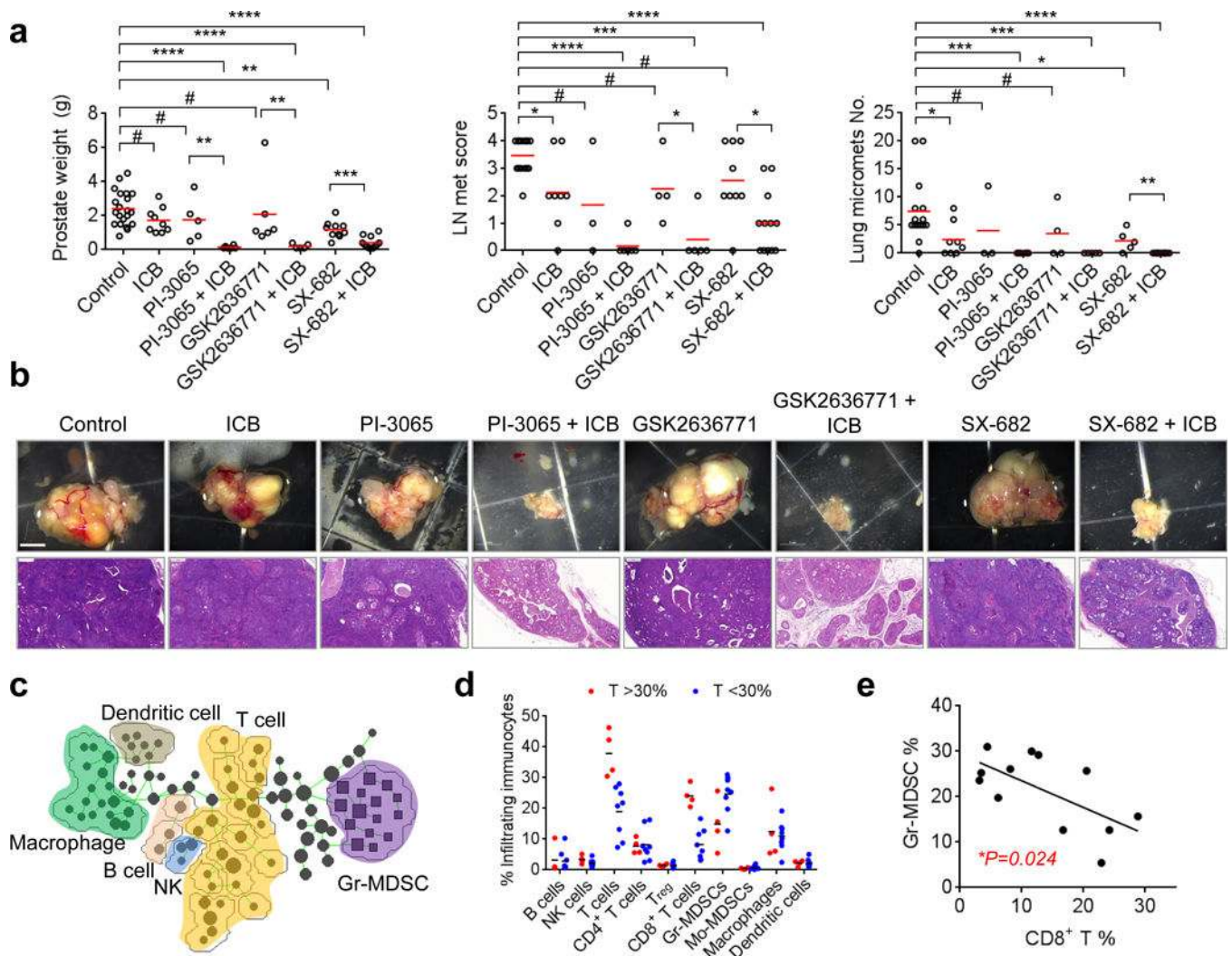
Figure 4. Gr-MDSCs inversely correlate with CD8$^+$ infiltrating T cells in human prostate cancer
(**a–b**) Efficacy of isoform-selective p110 inhibitors or Cxcr1/2 inhibitor as single agents or in combination with ICB to treat mCRPC in CPPSML model (n=15, 8, 3, 6, 4, 5, 5, and 10 respectively, biological replicates). Red bar indicates the mean. *P<0.05, **P<0.01, ***P<0.001, ****P<0.0001, #P>0.05, Mann-Whitney test. Scale bars: 3mm for organ images, 200μm for H&E images. (**c**) SPADE tree derived from CyTOF analysis of human samples. All live infiltrating immune cells (CD45$^+$) were used to construct the tree. (**d**) Frequency of infiltrating immune cell populations from patient samples. (**e**) Linear regression analysis of Gr-MDSC frequency with CD8$^+$ T cell frequency. In (**c–e**), n=12 (biological replicates).